2021

Analysis of Three-phase Rectifier via Three Different Control Methods and Switch Power Loss Comparison

Yichao Wang
Minnesota State University, Mankato

Analysis of Three-phase Rectifier via Three Different Control Methods and Switch Power Loss Comparison

By

Yichao Wang

A Thesis Submitted in Partial Fulfillment of the

Requirements for the Degree of

Master of Science

In

Electrical Engineering

Minnesota State University, Mankato

Mankato, Minnesota

July 2021

July 1st, 2021

Analysis of Three-phase Rectifier via Three Different Control Methods and Switch Power Loss Comparison

Yichao Wang

This thesis has been examined and approved by the following members of the student's committee.

_____
PROF. VINCENT WINSTEAD

_____
PROF. JIANWU ZENG

_____
PROF. HAN-WAY HUANG

Acknowledge

Thanks for all the help and instruction from my advisor Dr. Vincent Winstead and all the professors who instructed me.

ANALYSIS OF THREE-PHASE RECTIFIER VIA THREE DIFFERENT CONTROL METHODS AND SWITCH POWER LOSS COMPARISON

YICHAO WANG

A THESIS SUBMITTED IN PARTIAL FULFILLMENT OF THE

REQUIREMENTS FOR THE DEGREE OF

MASTER OF SCIENCE IN ELECTRICAL ENGINEERING

MINNESOTA STATE UNIVERSITY, MANKATO

MANKATO, MINNESOTA

JULY 2021

ABSTRACT

Traditional uncontrolled or phase-controlled rectifiers have the defects of lower power factor and nontrivial higher harmonics which causes the low efficiency of power, bad power quality, and so on. However, PWM rectifiers overcome the drawbacks mentioned above. They reduce the higher harmonics yielding better sinusoidal current on the grid side, achieve unity power factor and bidirectional power flow, and have better dynamic performance. So, it is favored more by academia and widely applied in high-performance power electronics devices. In this paper, the PWM rectifier is analyzed and a comparison of the switch loss on three-phase rectifier using three different control methods is completed in MATLAB / Simulink.

Analysis of the PWM rectifier includes analysis of the common topologies of the rectifier, the mathematical model of three-phase rectifier and control methods of three-phase rectifiers.

First, the common types and the corresponding topologies of the rectifier are analyzed. Second, the mathematical models of three-phase PWM rectifier are analyzed. In the general mathematical models, there are two types of models. One is based on a switch function and the other one is based on duty ratio. Furthermore, the mathematical model of three-phase rectifier in the d-p coordinate system is analyzed. Three different control methods on three-phase rectifiers are analyzed including hysteresis control, double-loop decoupling SPWM (Sinusoidal Pulse Width Modulation) control and double-loop decoupling SVPWM control. Then explained in detail is the SVPWM modulation principle and its realization.

The simulations of three different control methods on three-phase rectifiers are built in MATLAB / Simulink. The dynamic responses of the three different methods are shown. The switch model used in the simulation is introduced. Finally, the comparison of the power loss on the three different methods is completed.

Contents

Acronyms and Common Variables

PWM: Pulse-Width Modulation.

SVPWM: Space Vector Pulse Width Modulation.

SPWM: Sinusoidal Pulse Width Modulation.

VSR: Voltage-Source Rectifier.

MOSFET: Metal-Oxide Semiconductor Field-Effect Transistors.

$e\ (t)$: The AC side electromotive force.

$i_{ac}\ (t)$: The AC side current.

$v_{ac}\ (t)$: The AC side voltage.

$i_{dc}\ (t)$: The DC side current.

$i_L\ (t)$: The DC side load current.

$i_C\ (t)$: The DC side capacitor current.

$v_{dc}\ (t)$: The DC side voltage.

$e_L\ (t)$: The DC side electromotive force.

R_L: The DC side load.

L: Inductor.

E: Phasor, the AC side electromotive force.

V: Phasor, the AC side voltage.

I: Phasor, the AC side current.

V_L: Phasor, voltage over the AC side inductor.

Chapter 1 Introduction

1.1 Motivation

Today, electricity is one of the primary forms of energy used in human society worldwide. Common household appliances utilizing sub-distribution level voltage via transformers constitute a non-trivial load on electric grids. Power electronics is the application of solid-state electronics to the control and conversion of electric power[1], which is frequently used between grid and electric appliances. However, power factor and higher harmonics are two factors having great impact on the performance of load and efficiency of power consumption.

PWM based voltage rectification provides a methodology to facilitate electric conversion in power converters.

Electric power conversion is realized using power electronics. The power conversion system can be classified according to the type of the input and output power:

- AC to DC (rectifier)
- DC to AC (inverter)
- DC to DC (DC-to-DC converter)
- AC to AC (AC-to-AC converter)[1]

In 1957, the development of thyristors led to the birth of power electronics. Then during the next half century, other devices were developed such as SCR (Silicon Controlled Rectifier), BJT (Bipolar Junction Transistor), IGBT (Insulated Gate Bipolar Transistor) and MOSFET (Metal-Oxide-Semiconductor Field-effect Transistor), etc.[2]. We can see a trend in the development of power electronics switches: from half controlled to fully controlled. However, diodes and thyristors are usually selected as power electronics switches which yield uncontrolled rectification and half controlled rectification respectively. What comes along with this choice are the following consequences: power flow is not bi-directional, the volume of the rectifier is relatively larger, bad dynamic response. Moreover, there are impacts to the grid, e.g. it introduces substantial reactive power and higher current harmonics to the grid leading to a low input power factor on the grid side and causes even more problems to the grid as follows[2]:

(1) It increases reactive power loss in the power grid, causes overheating of equipment and lines thereby shortening the life of power grid equipment; Meanwhile there will be a large neutral line current, which reduces the safety and stability of power grid equipment and causes resonance in the power grid, affecting the normal power supply system. If the situation is serious, the power grid may collapse.

(2) It has an impact on voltage transformers, cables, motors, and other equipment, and may even damage the equipment in severe cases. In addition, it may cause the malfunction of automatic devices of electronic components, making electronic

instruments or communication equipment malfunction, and reduce communication quality, etc.

Furthermore, the current harmonics in the power grid will propagate with the flow of energy, thereby affecting other electrical devices and causing many problems to the power transmission and distribution system. Regarding these effects of current harmonics in the power grid, IEEE (Institute of Electrical and Electronics Engineers), IEC (International Electrotechnical Commission) and CIGRE (International Council on Large Electric Systems) have proposed standards with specific restrictions on power factor and waveform distortion of electrical devices separately[2].

To address the issue of low power factor and higher harmonics, usually one can apply the following strategies:

(1) Compensating for the harmonics. LC filter or active power filter are frequently used in the case.
(2) Improving the electric power conversion. PWM rectifier is one possible methodology.

1.2 Overview of PWM Rectifier

As fully controlled power electronic switches (e.g. IGBT) technology became more and more mature and were applied in more applications, this boosted the development of PWM technology. In 1979, T Kataoka, et al published *A "pulse-width controlled AC-to-*

DC converter to improve power factor and waveform of AC line current" where the concept of PWM control was introduced for the first time[3]. Soon after, Alfred Busse and Joachim Holtz pioneered in optimal rectifier topologies and introduced the three-phase full bridge consisting of fully controlled power electronics switches achieving unity power factor operation with sinusoidal input current on the AC side[4]. In 1984, Akagi Hirofumi et al introduced a control strategy for reactive power compensator based PWM rectifier[5]. In the subsequent years, scholars focused on mainly the improvement of the control algorithm for PWM rectifiers. Among them was A. W. Green who proposed to discretize the mathematical models of PWM rectifiers in different coordinate systems, and gave the corresponding control algorithms as a prelude to developing the theory of PWM rectifier control[6].

There are many criteria to categorize PWM rectifiers. Among them there is a basic criterion in which they are categorized by how the energy is stored in the DC side[7]. There exists two main categories: voltage type and current source type. In the former, a capacitor is used to store energy providing a smooth voltage and it is an equivalent low resistance voltage source on the DC side. In the latter, an inductor is used to store energy providing a smooth current. It is an equivalent high resistance current source on the DC side.

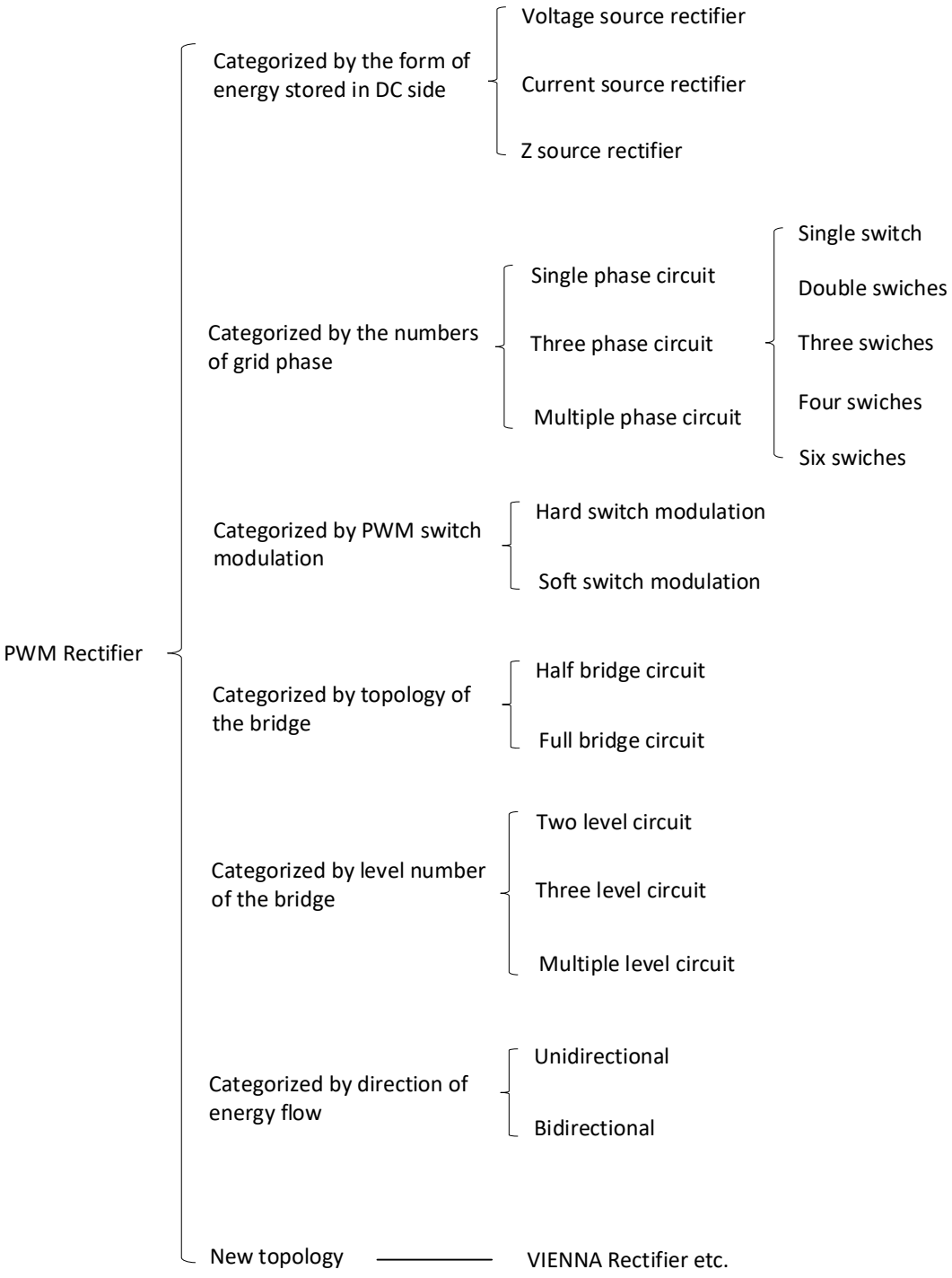

Figure 1.1 Category of Rectifier[8]

1.3 Control strategy of PWM Rectifier

There are two main aims in the control of a PWM rectifier:

(1) Maintaining the requested voltage level, especially when a disturbance occurs in voltage or there is a disturbance from the change of load.

(2) Achieving sinusoidal current on the AC side and unity power factor.

According to whether the control strategy has an inner current loop or not, the control strategy of PWM rectifier is classified to two main categories:

(1) Indirect current control.

(2) Direct current control.

In indirect current control, there is a closed loop control for the voltage, and what is directly controlled is the voltage on the AC side. This is achieved by letting the controlled voltage satisfy some relationship with voltage on the grid side with respect to phase and amplitude[8]. Consequently we get the desired current on the AC side. However, in direct current control, the set point current is given by the output of the voltage closed loop, by sampling and comparing the real current with the set point current we can build the inner current closed loop. Compared with direct current control indirect current control requires a simpler control logic, however direct current control has better dynamic response so that the voltage can return to the desired set point level more quickly after an exterior disturbance or load change. The double closed loop design in direct current

control sacrifices simplicity gaining better control characteristics on the rectifier. This has become a more popular control method. In direct current control, the outer voltage loop is used to smooth the voltage on the DC side. Here the PI (proportional and integral) control is used. Nevertheless, a change in parameters for the rectifier and the disturbance from the load can degrade the control performance. Moreover, the outer voltage loop has a poor dynamic response. To address the issue mentioned above, we can use the square of voltage magnitude as the manipulated variable instead of voltage as in traditional PI control to achieve the linearized outer voltage loop control. This leads to the enhancement of the dynamic characteristics and the robustness against disturbances[8]. In inner current loop, we track the phase of the voltage on the grid side and aim to get a sinusoidal current as much as possible to achieve unity power factor. Because the inner current loop determines the dynamic characteristics and robustness of the controller, research on the inner current loop is necessary. Compared with analog control digital control based on MCU (Microcontroller Unit), DSP (Digital Signal Processor), FPGA (Field-Programmable Gate Array) etc. is more flexible. Prior to the broad adoption of digital control technology, analog control was usually adopted in early PWM rectifier control, more recently, as the performance of the digital controller has experienced enhancements, digital control methods have dominated the literature[9]. If we regard the control strategy on inner current loop as the criterion in VSR (Voltage Source Rectifier), the control strategies of VSR are classified as follows:

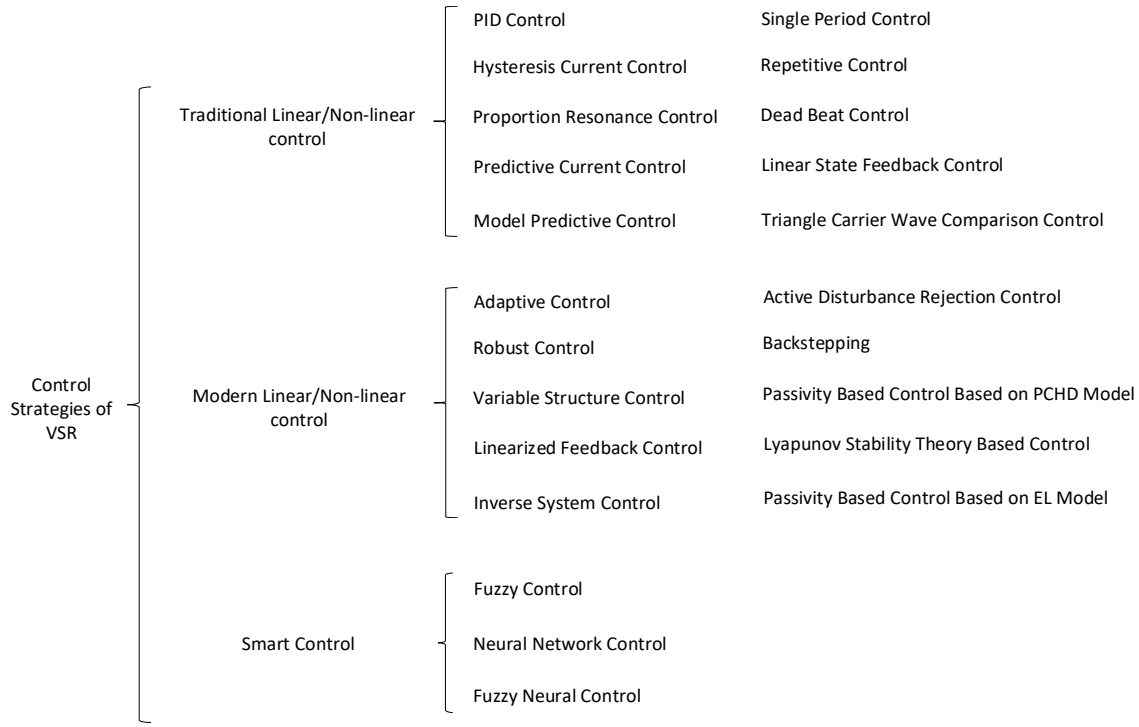

Figure 1.2 Classification of VSR Control[8]

1.4 Modulation Method

There are two common modulation methods of PWM rectifier: SPWM (Sinusoidal Pulse Width Modulation) and SVPWM (Space Vector Pulse Width Modulation). SPWM was widely applied early and therefore a mature technology, which is easy to realize. When the carrier wave frequency is high enough and the SPWM method is adopted, the output wave is a standard sinusoidal wave, which is a good candidate for the drive signal of an IGBT or MOSFET. Moreover the higher harmonics also get suppressed. But when the carrier wave frequency is lower, the output wave is no longer standard sinusoidal. Instead

we can only get a very distorted quasi sinusoidal wave. On one hand, the logic of SVPWM is complex. On the other hand, SVPWM currently has the best performance of higher harmonics suppression. Furthermore, compared with traditional PWM, SVPWM achieves better output voltage utilization rate on the DC side, has less power loss on power switches and merits a better robustness. LC filters can well suppress the higher harmonic spike when the switching frequency of PWM rectifier is between 3-15 KHz. However, once the switching frequency is too high, an LC filter is not able to handle the higher harmonic spike. Regarding the issue mentioned above, an LCL filter proposed in 1988, by M. Lindgren et al. addresses the problem effectively[9].

Chapter 2 Model of Three-Phase PWM Rectifier

2.1 Overview of PWM Rectifier

The rectifier is one of the earliest used converter devices in the development of power electronics. Starting from uncontrolled rectification, phase-controlled rectification to the current stage of PWM rectification has much better performance compared with earlier rectification methods. The combination of fully controlled semi-conductor, chopper control and PWM rectifier is a breakthrough. Compared with the early-stage uncontrolled semi-conductor switching device (mainly freewheeling diode) rectification method and semi-controlled semiconductor switching device (mainly thyristor) rectification method, PWM rectification method mainly has the following 4 advantages[10]:

(1) The grid-side current and voltage both show sine wave characteristics, and the current is in phase with voltage.
(2) Controllable grid-side power factor and unity power factor operation.
(3) Bidirectional power flow between the grid side and the DC side.
(4) Fast dynamic response.

There are two modes of operation of the PWM converter which can be realized via the control of the fully controlled device (on or off): When absorbing power from the grid,

it is operating in the mode of rectification; When transmitting power to the grid, it is operating in the mode of active inverter. The unity power factor mentioned above is defined by that when operating in the mode of rectification, voltage is in phase with current (Positive resistance characteristics) on the grid side. When operating in the mode of inverter, voltage has inverted phase with respect to current (Negative resistance characteristics) on the grid side.

Further studies in the literature demonstrate that the current and power factor of PWM converter are both controllable on the grid side. This is demonstrated through APF (Active power filter), SVC (static var compensator), etc. converter applications.

Figure 2.1 is the circuit topology of the PWM rectifier model.

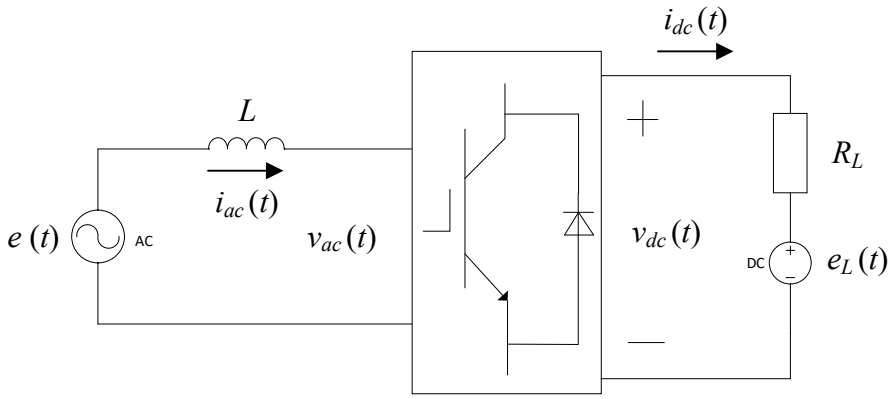

Figure 2.1 Topology of PWM Rectifier Model[11]

As shown in Figure 2.1 we see there are 3 main components of the PWM rectifier: AC circuit, power switch bridge and DC circuit. Ignoring the power loss on switches and

according to the law of conservation of energy, the power on the AC circuit side equals the power on DC circuit side. Therefore we can write:

$$v_{ac}(t)\, i_{ac}(t) = v_{dc}(t)\, i_{dc}(t) \tag{2-1}$$

where $v_{ac}(t)$ and $i_{ac}(t)$ are the voltage and current on the AC side of the model and $v_{dc}(t)$ and $i_{dc}(t)$ are the voltage and current on the DC side of the model.

According to equation (2-1) , we know that we can control current and voltage on the DC side by controlling current and voltage on the AC side, and vice versa. When in the steady state, the relationship of the vectors on the AC side is shown in Figure 2.2 and more detailed explanation on it is developed as follows:

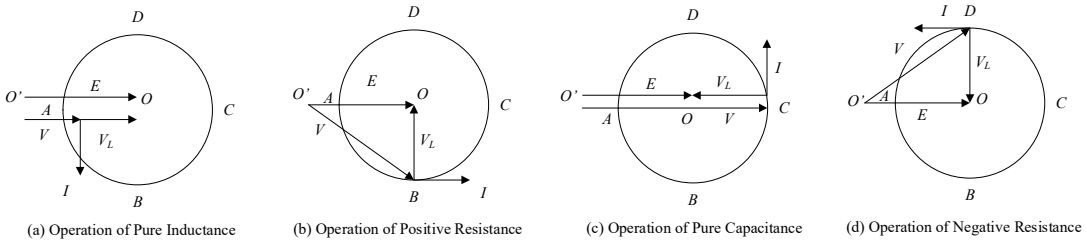

Figure 2.2 Relationship of Vectors in Steady State on the AC Side of PWM Rectifier[12]

To simplify the analysis, we only consider the fundamental harmonic and we ignore the resistance on the AC side. Below is the analysis on the operation status and the principle of control:

When taking the grid electromotive force vector as a reference, the four-quadrant operation of the rectifier can be realized by controlling the AC voltage vector. Assuming the absolute value $|I|$ is constant, then $|V_L| = \omega L|I|$ is also constant. In this case, the trajectory of the end point of the AC voltage vector of the PWM rectifier forms a circle with a radius of $|V_L|$. When the end point of the voltage vector V (this vector and the vectors mentioned in the analysis of the relationship of the vectors on the AC side are all phasors) is at the point A of the circle, the current vector I is 90 degrees behind than the generator electromotive force vector E (which is simulated by the sine wave in the simulation in Chapter 4), and the rectifier grid side presents pure inductance characteristics at this time, as in Figure 2.2 (a); When the voltage vector goes to point B of the circle, the current vector I is in parallel with electromotive force vector E, PWM rectifier grid side presents characteristics of pure resistance at the this time, as in Figure 2.2 (b); When the voltage vector goes to point C, the current vector I is 90 degrees forward than electromotive force vector E, PWM rectifier grid side presents characteristics of pure capacitance at the this time, as in Figure 2.2 (c); When the voltage vector goes to point D, the current vector I and electromotive force vector E are antiparallel, PWM rectifier grid side presents characteristics of negative resistance at this time, as in Figure 2.2 (d).

The four points A, B, C, D mentioned above are special operation points, we can conclude that the rules in the four-quadrant operation of PWM rectifier as follows:

1) When voltage vector V is moving down arc AB, PWM is operating in the mode of rectification where the PWM rectifier absorbs active power and inductive reactive power from the grid and transmits power via the rectifier to a DC load. When the rectifier is operating at point B, it achieves unity power factor, whereas when operating at point *A*, PWM rectifier only absorbs inductive reactive power rather than active power from the grid.

2) When voltage vector V is moving down arc BC, PWM is operating in the mode of rectification where the PWM rectifier absorbs active power and capacitive reactive power from the grid and transmits power via the rectifier to a DC load. When the rectifier is operating at point C, PWM rectifier only absorbs capacitive reactive power rather than active power from the grid.

3) When voltage vector V is moving down arc CD, PWM is operating in the mode of active inverter where the PWM rectifier transmitting active power and capacitive reactive power to the grid from the DC side. Especially when PWM rectifier reaches point *D*, unity power factor is achieved.

4) When voltage vector V is moving down arc DA, PWM is operating in the mode of active inverter where the PWM rectifier transmitting active power and inductive reactive power to the grid from the DC side.

According to the analysis above, we can achieve the four-quadrant operation of the rectifier with controllable power factor by controlling the current on the grid side. We can

control the current indirectly by controlling the voltage on the grid side or we can control the current by a closed-loop method directly. And the control methods mentioned here are indirect current control and direct current control respectively[13].

2.2 Topology of PWM Rectifier

2.2.1 Topology of voltage-source PWM rectifier

1) Single-phase voltage-source PWM rectifier

The topology of a single-phase voltage-source PWM rectifier is shown in Figure 2.3, where (a), (b) are single-phase half bridge PWM rectifier and single-phase full bridge PWM rectifier respectively. The AC sides are identical where the inductor is used for filtering out the harmonics on the grid side.

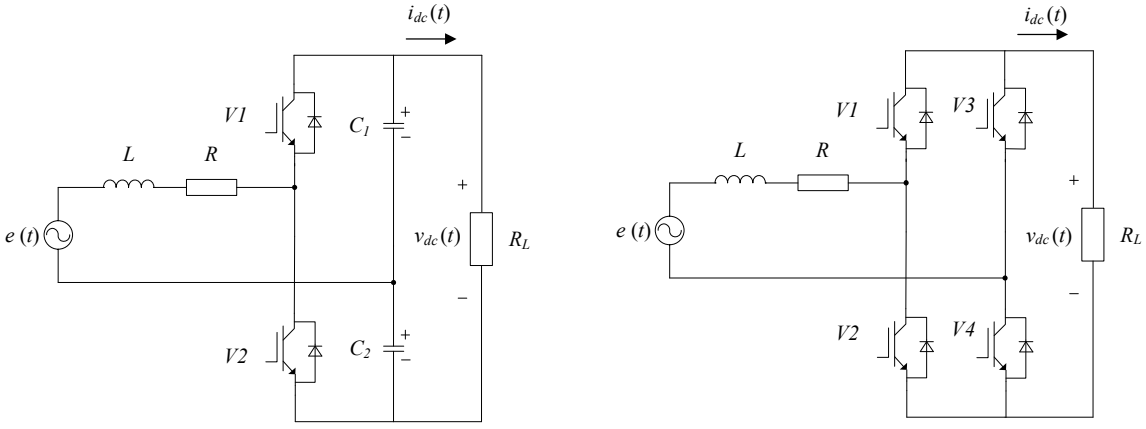

(a) Single-phase half bridge PWM rectifier

(b) Single-phase full bridge PWM rectifier

Figure 2.3 Single-phase voltage source PWM rectifier topology[14]

As seen in Figure 2.3 (a), there are two power switches in only one of the bridge arms and in another it comprises two capacitors, which are also used for storing energy on the DC side. In single-phase full-bridge rectifier, an H bridge circuit is adopted. By comparison, single-phase half bridge rectifier bears a simpler circuit and less power switches leading to a lower cost. Nevertheless, to have the same control characteristics of current on the AC side with the same circuit parameters of the AC side, the voltage on the DC side needs to be twice as much as in single-phase full-bridge rectifier, as a consequence, increasing the voltage stress of power switches. Furthermore, to maintain a smooth mid-point voltage of the two capacitors, voltage equalizing measurement should be adopted, which introduces complicated control issues to the implementation.

2) Three-phase voltage source type PWM rectifier

The topologies of three-phase voltage source type PWM rectifier are shown in Figure 2.4, in which (a), (b) are three-phase half bridge PWM rectifier and three-phase full bridge rectifier respectively and where the DC sides are identical. A three-phase symmetric connection is adopted in three-phase half bridge PWM rectifier with 6 power switches, which is a popular structure in three-phase PWM rectifier topology and applies well to three-phase symmetric power systems, however bearing the characteristics of strong coupling, strong nonlinearity and high complication in control. Moreover, its performance will degrade rapidly, and it may not even work at all when grid three-phase voltage is asymmetric. In order to overcome the drawback, an alternative is a three-phase full

bridge PWM rectifier that has 3 separately controlled single-phase full bridge PWM rectifier connecting to the grid via transformer. However due to its big volume and high cost it has less utility compared to the three-phase half bridge PWM rectifier[15]-[18].

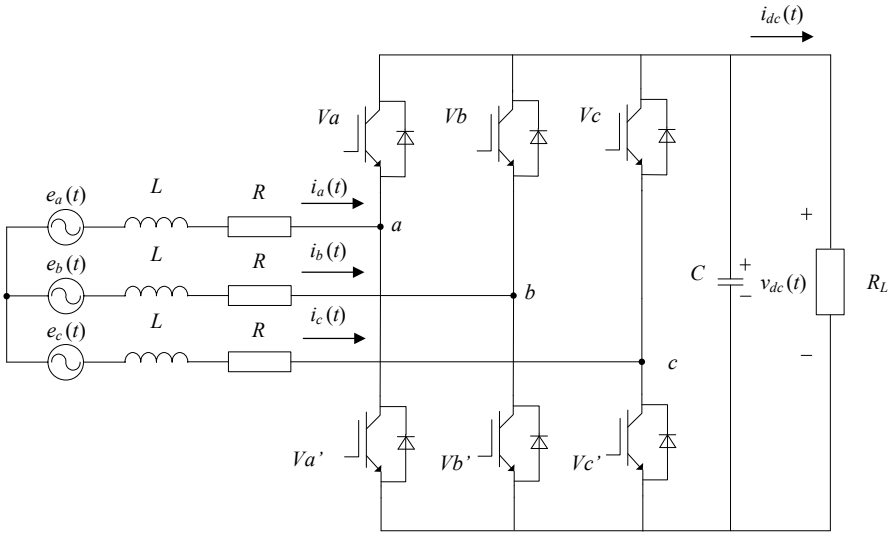

(a) Three-phase half bridge PWM rectifier

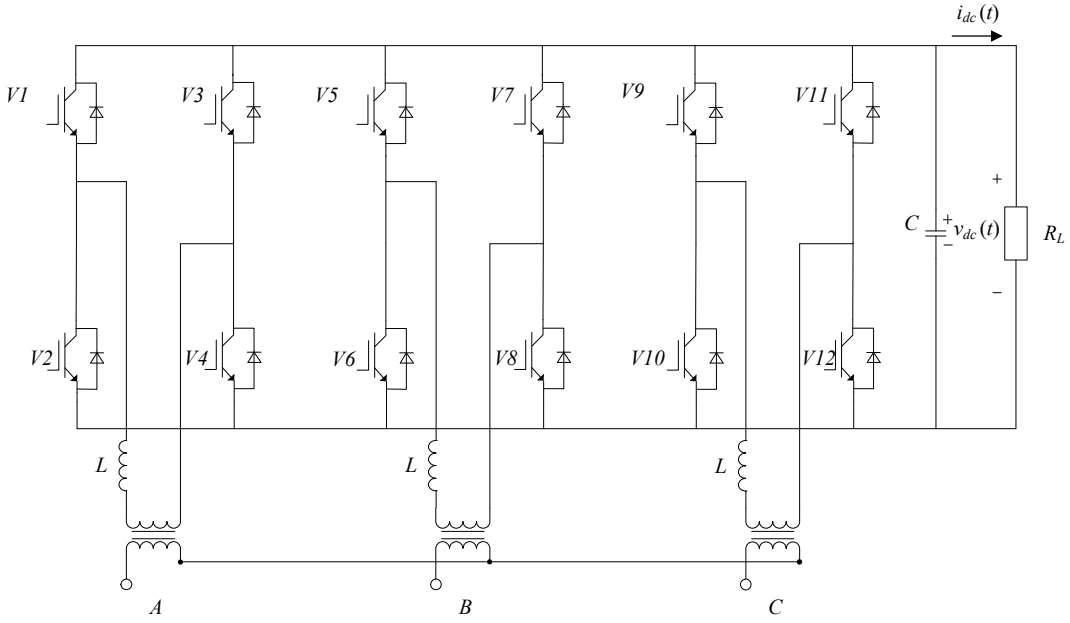

(b) Three-phase full bridge PWM rectifier

Figure 2.4 Topology of three-phase PWM rectifier[19]

2.2.2 Topology of current-source PWM rectifier

As is shown in Figure 2.5, a single-phase current source PWM rectifier has an inductor on the DC side compared with single-phase voltage source PWM rectifier and also has a filter capacitor on the AC side along with the inductor as a LC filer in order to filter out harmonic current on the grid side and suppress harmonic voltage on the AC side. In addition, diodes are usually in forward series with the power switch, so as to block reverse current and enhance the reserve voltage withstand of the power switch at the same time.

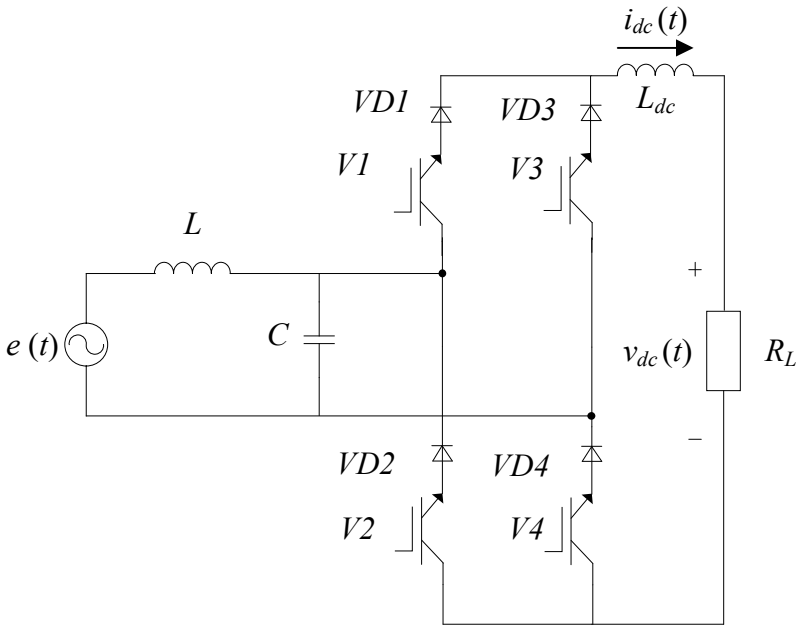

Figure 2.5 Topology of single-phase current source PWM rectifier[19]

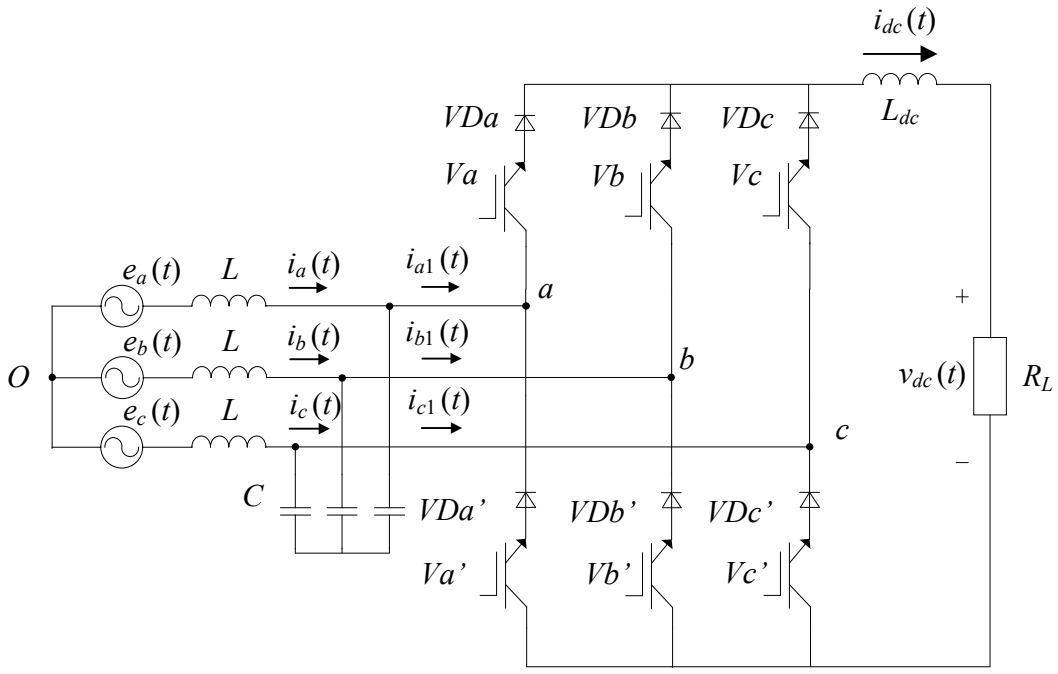

Figure 2.6 Topology of three-phase current source PWM rectifier[19]

As shown in Figure 2.6, a three-phase current source PWM rectifier topology, which is a half bridge circuit with a no mid wire three-phase symmetric LC filter circuit on the AC side. Similar to the DC side of the single-phase PWM rectifier, an inductor is adopted for energy storage. However, the complexity of the control complicates the analysis and application of current source PWM rectifier.

2.3 Mathematical Model of Three-Phase Voltage Source PWM Rectifier

2.3.1 A general mathematical model of three-phase voltage source rectifier (VSR)

A general mathematical model of a voltage source rectifier mentioned above refers to a general mathematical description of a three-phase voltage source rectifier in three-phase static coordinate system phases (a, b, c) according to its topology based on basic circuit laws (Kirchhoff's current law and Kirchhoff's voltage law). The topology of a three-phase voltage source rectifier with phases labeled is shown in Figure 2.7.

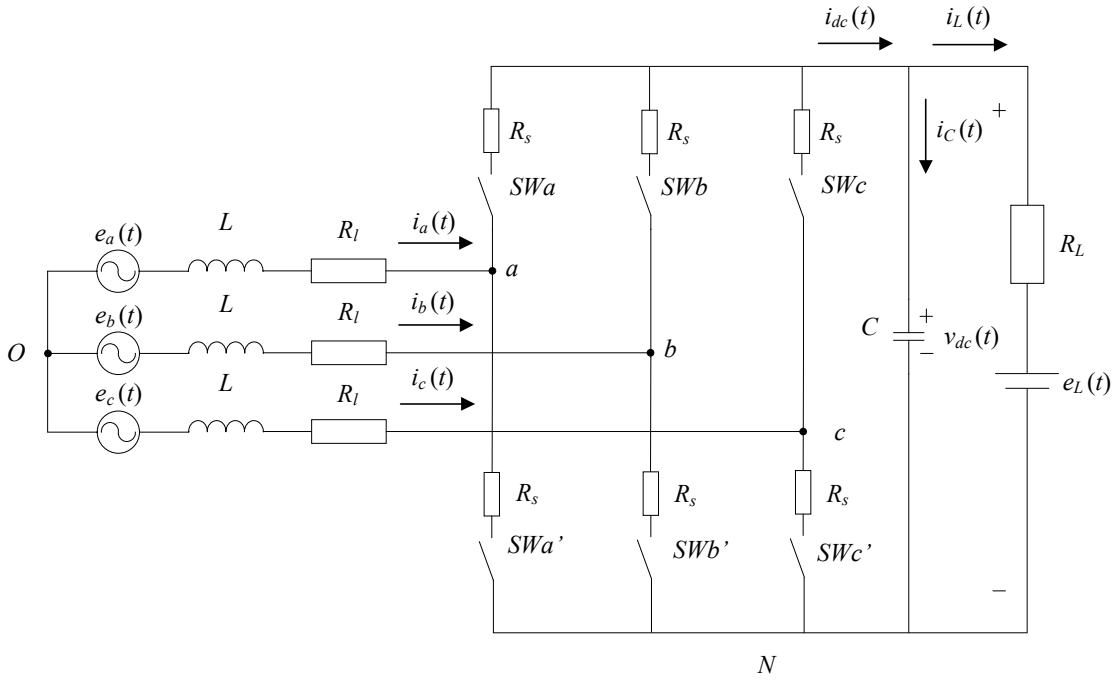

Figure 2.7 Mathematical model of three-phase VSR[20]

Usually, we have some assumptions constraining the general mathematical model of a three-phase voltage source rectifier as below:

(1) A three-phase ideal sinusoidal symmetric electromotive force source with individual RMS values (e_a, e_b, e_c).

(2) A linear grid side filter inductor without saturation.

(3) An equivalent per phase resistance R_s accounting for the power loss of the power switches. That is, we model the power switch as an ideal switch in series with a loss resistance R_s.

(4) In order to imitate the bi-directional transmission of the power of the three-phase voltage source rectifier, the DC side load comprises a resistance R_L in series with an ideal DC electromotive force (DC voltage supply).

According to needs in different aspects, we can build two general mathematical models of a three-phase voltage source rectifier in different forms as follows:

(1) A general mathematical model based on switch function.

(2) A general mathematical model based on duty ratio.

A general mathematical model based on switch function describes the process of switching of voltage source rectifier (VSR) precisely, which is good at the emulation of VSR waves. However, higher harmonics are introduced by the switching process when adopting the general mathematical model based on switch function. The general mathematical model based on a duty ratio is, in contrast, suitable for analyzing the control system as well as for designing the controller directly. The general mathematical model based on duty ratio is a simplified version of the general mathematical model based on switch function, which only concerns the low frequency component ignoring the higher harmonics in the general mathematical model based on switch function. This holds

assuming the switching frequency is much higher than the first harmonic in the grid waveforms. On the other hand, it is not able to emulate the dynamics not accounting for the higher harmonics in the switching process. In essence, the general mathematical model based on switch function and the general mathematical model based on duty ratio play important roles respectively on their own merits in emulating systems and designing controllers. Usually, we adopt the latter to design the controller and then apply the former to the emulation of the control system so that we can verify the characteristics of the control system.

2.3.1.1 A general mathematical model of VSR based on switch function[20]

Referring to three-phase VSR, we build the general mathematical model based on switch function.

As in Figure 2.7, when DC electromotive force $e_L(t) = 0$, we have a purely resistive load on the DC side. In this scenario the three-phase VSR can only operate in rectification mode. When $e_L(t) > v_{dc}(t)$, three-phase VSR can either operate in rectification mode or active inverter mode. Three-phase VSR transmits the power on $e_L(t)$ from the DC side to the grid when operating in active inverter mode, which is also called regenerative power generation mode. When $e_L(t) < v_{dc}(t)$ the three-phase VSR can only operate in rectification mode.

For the sake of convenience of analysis, we define the boolean switch function s_k of three-phase rectifier power switch as below:

$$s_k = \begin{cases} 1; & \text{The upper arm switch is turned on, and the lower arm switch is turned off} \\ 0; & \text{The upper arm switch is turned off, and the lower arm switch is turned on} \end{cases} \quad (2\text{-}2)$$

Where $k \in \{a,b,c\}$.

We merge three-phase VSR power switch loss resistance R_s with equivalent loss resistance R_l as R, so $R = R_s + R_l$. Then apply Kirchhoff's voltage law (KVL) to build three-phase VSR circuit formula in phase a:

$$L\frac{di_a}{dt} + Ri_a = e_a - (v_{aN} + v_{NO}) \quad (2\text{-}3)$$

where $v_{NO} = v_N - v_O$ the voltage between point N and point O in Figure 2.7. When SWa is turned on and SWa' is turned off, $s_a = 1$ and $v_{aN} = v_{dc}$. When SWa is turned off and SWa' is turned on, $s_a = 0$ and $v_{aN} = 0$. Since $v_{aN} = v_{dc}s_a$, equation (2-3) can be modified to:

$$L\frac{di_a}{dt} + Ri_a = e_a - (v_{dc}s_a + v_{NO}) \quad (2\text{-}4)$$

The same for phases b and c:

$$L\frac{di_b}{dt} + Ri_b = e_b - (v_{dc}s_b + v_{NO}) \tag{2-5}$$

$$L\frac{di_c}{dt} + Ri_c = e_c - (v_{dc}s_c + v_{NO}) \tag{2-6}$$

Given a three-phase symmetric system, we have

$$e_a + e_b + e_c = 0; \qquad i_a + i_b + i_c = 0 \tag{2-7}$$

Combining equations (2-4) ~ (2-7) , so

$$v_{NO} = -\frac{v_{dc}}{3}\sum_{k\in\{a,b,c\}} s_k \tag{2-8}$$

In Figure 2.7, It holds true that there is always one power switch turned on in one bridge arm, so there are 2^3 = 8 switching combinations in total. Hence, we can describe i_{dc} on the DC side as:

$$\begin{aligned} i_{dc} &= i_a s_a \overline{s}_b \overline{s}_c + i_b s_b \overline{s}_c \overline{s}_a + i_c s_c \overline{s}_b \overline{s}_a + (i_a + i_b) s_a s_b \overline{s}_c \\ &\quad + (i_a + i_c) s_a s_c \overline{s}_b + (i_b + i_c) s_b s_c \overline{s}_a + (i_a + i_b + i_c) s_a s_b s_c \\ &= i_a s_a + i_b s_b + i_c s_c \end{aligned} \tag{2-9}$$

In addition, applying Kirchhoff's current law at the positive node of the capacitor, yields

$$C\frac{dv_{dc}}{dt} = i_a s_a + i_b s_b + i_c s_c - \frac{v_{dc} - e_L}{R_L} \tag{2-10}$$

Combining equations (2-4) - (2-10) , and using a state variable X with $X = [i_a \quad i_b \quad i_c \quad v_{dc}]^{\mathrm{T}}$, yields an expression for the system of the general mathematical model of three-phase VSR described by unipolar binary logic switch function as follows:

$$Z\dot{X} = AX + BE \tag{2-11}$$

where

$$A = \begin{bmatrix} -R & 0 & 0 & -\left(s_a - \frac{1}{3}\sum_{k\in\{a,b,c\}} s_k\right) \\ 0 & -R & 0 & -\left(s_b - \frac{1}{3}\sum_{k\in\{a,b,c\}} s_k\right) \\ 0 & 0 & -R & -\left(s_c - \frac{1}{3}\sum_{k\in\{a,b,c\}} s_k\right) \\ s_a & s_b & s_c & -1/R_L \end{bmatrix} \tag{2-12}$$

$$Z = \begin{bmatrix} L & 0 & 0 & 0 \\ 0 & L & 0 & 0 \\ 0 & 0 & L & 0 \\ 0 & 0 & 0 & C \end{bmatrix} \tag{2-13}$$

$$B = \begin{bmatrix} 1 & 0 & 0 & 0 \\ 0 & 1 & 0 & 0 \\ 0 & 0 & 1 & 0 \\ 0 & 0 & 0 & \frac{1}{R_L} \end{bmatrix} \tag{2-14}$$

$$E = \left[e_a \; e_b \; e_c \; e_L \right]^{\mathrm{T}} \tag{2-15}$$

2.3.1.2 A general mathematical model of VSR based on duty ratio[20]

In order to exclude the higher frequency component described in the general mathematical model of VSR based on a switch function, we expand the switch function with Fourier Series form. The Fourier Series for any periodic function is as below:

$$f(\omega t) = a_0 + \sum_{n=1}^{\infty} a_n \sin(n\omega t) + \sum_{n=1}^{\infty} b_n \cos(n\omega t) \tag{2-16}$$

If we use a triangle shaped modulation wave in PWM control, when natural sampling is adopted to generate the PWM signal, the switching waveform is shown in Figure 2.8 (a), where the switching waveform is not symmetric in one switching period. However, when the switching frequency is far greater than the grid frequency, we can adopt regular sampling rather than natural sampling. When regular sampling is applied, as shown in Figure 2.8 (b), obviously, the switching waveform is symmetric over one switching period.

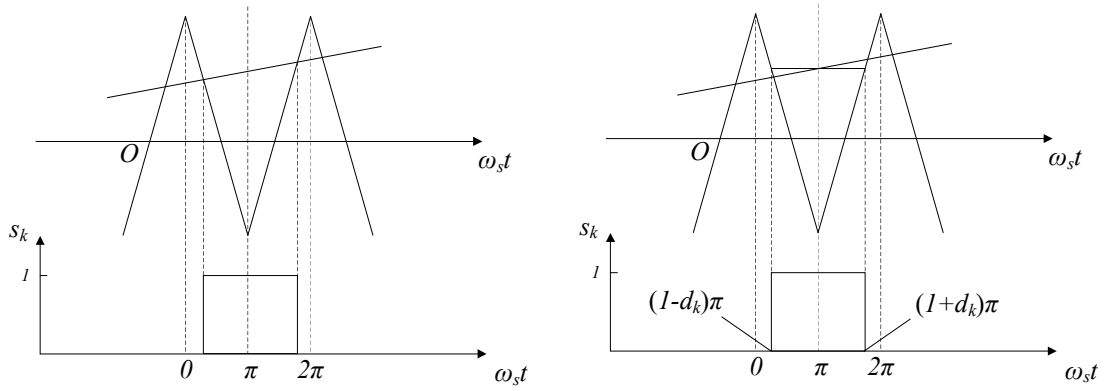

(a) Natural Sampling (b) Regular Sampling

Figure 2.8 PWM and waveform of switch function

In Figure 2.8, $\omega_s = 2\pi f_s$, where f_s is the PWM switching frequency, d_k is the corresponding duty ratio, and $d_k \le 1$.

In Figure 2.8 (b), the relationship between switch function s_k and duty ratio d_k is as follows:

$$s_k = \begin{cases} 0;\ 0 \le \omega_s t < (1-d_k)\pi, (1+d_k)\pi < \omega_s t \le 2\pi \\ \\ 1;\ (1-d_k)\pi \le \omega_s t \le (1+d_k)\pi \end{cases} \tag{2-17}$$

where $k \in \{a,b,c\}$.

According to Figure 2.8 and relationship above, it shows that d_k is actually the average of the switch function s_k in one switching period. Therefore,

$$a_0 = \frac{1}{2\pi}\int_{(1-d_k)\pi}^{(1+d_k)\pi} s_k \, d(\omega_s t) = d_k \tag{2-18}$$

$$\begin{cases} a_n = 0 \\ b_n = (-1)^n \dfrac{2}{n\pi}\sin(nd_k\pi) \end{cases} \tag{2-19}$$

$$s_k = d_k + \sum_{n=1}^{\infty}(-1)^n \frac{2}{n\pi}\sin(nd_k\pi)\cos(n\omega_s t) \tag{2-20}$$

It follows that

$$\sum_{k\in\{a,b,c\}} s_k = \sum_{k\in\{a,b,c\}} d_k + \sum_{n=1}^{\infty}\left[\sum_{k\in\{a,b,c\}}(-1)^n \frac{2}{n\pi}\sin(nd_k\pi)\right]\cos(n\omega_s t) \tag{2-21}$$

Combining equation (2-20) , equation (2-21) and equation (2-12) yields

$$A = A_l + A_h \tag{2-22}$$

where A_l —— low frequency component in matrix A ;

A_h —— high frequency component in matrix A .

and

$$A_l = \begin{bmatrix} -R & 0 & 0 & -\left(d_a - \frac{1}{3}\sum_{k\in\{a,b,c\}} d_k\right) \\ 0 & -R & 0 & -\left(d_b - \frac{1}{3}\sum_{k\in\{a,b,c\}} d_k\right) \\ 0 & 0 & -R & -\left(d_c - \frac{1}{3}\sum_{k\in\{a,b,c\}} d_k\right) \\ d_a & d_b & d_c & -1/R_L \end{bmatrix} \tag{2-23}$$

$$A_h = \begin{bmatrix} 0 & 0 & 0 & A_{a4} \\ 0 & 0 & 0 & A_{b4} \\ 0 & 0 & 0 & A_{c4} \\ A_{4a} & A_{4b} & A_{4c} & 0 \end{bmatrix} \tag{2-24}$$

where

$$\begin{aligned} A_{k4} &= -\sum_{n=1}^{\infty}\left\{(-1)^n \frac{2}{n\pi}\left[\sin(nd_k\pi) - \frac{1}{3}\sum_{k\in\{a,b,c\}}\sin(nd_k\pi)\right]\cos(n\omega_s t)\right\} \\ A_{4k} &= -\sum_{n=1}^{\infty}\left[(-1)^n \frac{2}{n\pi}\sin(nd_k\pi)\cos(n\omega_s t)\right] \qquad (k \in \{a,b,c\}) \end{aligned} \tag{2-25}$$

Corresponding to $A = A_l + A_h$. The state variable X comprises higher frequency component X_h and lower frequency component X_l . That is,

$$X = X_l + X_h \tag{2-26}$$

According to equation (2-11) , we can conclude that the general mathematical model of three-phase VSR based on duty ratio is:

$$Z(\dot{X}_l + \dot{X}_h) = (A_l + A_h)(X_l + X_h) + BE \tag{2-27}$$

where, the lower frequency mathematical model is:

$$Z\dot{X}_l = A_l X_l + BE \tag{2-28}$$

the higher frequency mathematical model is:

$$Z\dot{X}_h = A_h X_l + A_l X_h + A_h X_h \tag{2-29}$$

Obviously, we can get the lower frequency mathematical model of three-phase VSR based on duty ratio by eliminating the higher frequency component in equation (2-27). Consequently, the lower frequency model simplifies the analysis and design of the three-phase VSR control system.

2.3.2 The dq model of three-phase VSR

We have introduced the mathematical model of three-phase VSR in a three-phase symmetric static coordinate system as above. Although it has a clear physics meaning and appears to be intuitive, all the quantities on the AC side are time-varying AC quantities, which makes it complicated to design the control system. Therefore, we can transfer the three-phase symmetric static coordinate system to a rotary coordinate system that is rotating at the same speed with the first harmonic in the three-phase symmetric static coordinate system. After we transform the phasors from the three-phase symmetric

static coordinate system to the DC variables in a dq coordinate rotating at the same speed with first harmonic, it becomes easier to design the control system. We can get the dq mathematical model by transferring the variables of the general mathematical model of three-phase VSR from three-phase symmetric static coordinate system to dq coordinate system rotating at the same speed of the first harmonic in three-phase symmetric coordinate system.

There are two kinds of coordinate system transformations usually involved in building the dq mathematical model of three-phase VSR. The first kind involves transforming the three-phase symmetric coordinate system (a,b,c) to two-phase static perpendicular coordinate system (α,ß). The other kind involves transforming the three-phase symmetric coordinate system (a,b,c) to two-phase synchronously rotating coordinate system (d,q), or transforming two-phase static perpendicular coordinate system (α,ß) to two-phase synchronously rotating coordinate system (d,q).

Here we use current $i(t)$ as an example to explain the equivalent transformation.

First, we define $i_0(t)$ as follows:

$$i_0(t) = \frac{1}{3}\left(i_a(t) + i_b(t) + i_c(t)\right) \tag{2-30}$$

1. Transformation from (a, b, c) to (α, ß, 0)

As shown in Figure 2.9, all axes share the common endpoint O. Axis a is aligned with axis α. The three axes a, b and c are aligned with a 120-degree difference sequentially. Axis β is 90 degrees ahead of axis α counterclockwise.

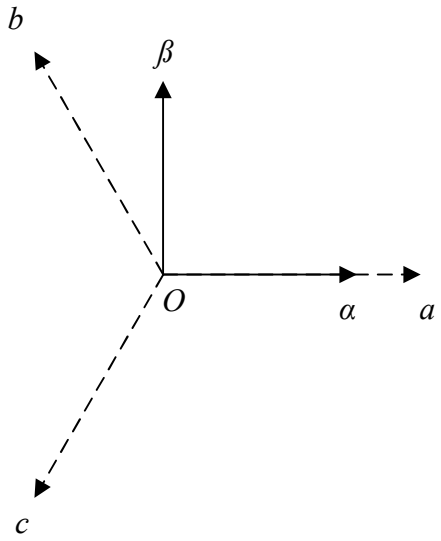

Figure 2.9 Alignment of (a, b, c) coordinate system and (α, ß) coordinate system

Here we do an Alpha–beta transformation as in equation (2-31) [21] to do the transformation.

$$\begin{bmatrix} i_\alpha(t) \\ i_\beta(t) \\ i_0(t) \end{bmatrix} = T \begin{bmatrix} i_a(t) \\ i_b(t) \\ i_c(t) \end{bmatrix} = \frac{2}{3} \begin{bmatrix} 1 & -\frac{1}{2} & -\frac{1}{2} \\ 0 & \frac{\sqrt{3}}{2} & -\frac{\sqrt{3}}{2} \\ \frac{1}{2} & \frac{1}{2} & \frac{1}{2} \end{bmatrix} \begin{bmatrix} i_a(t) \\ i_b(t) \\ i_c(t) \end{bmatrix} \quad (2\text{-}31)$$

2. Transformation from (α, ß, 0) to (d, q, 0)

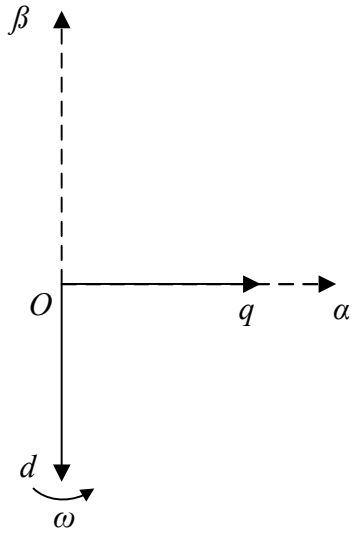

Figure 2.10 Alignment of (α, ß) coordinate system and (d, q) coordinate system

As shown in Figure 2.10, all axes share the common endpoint O, axis α is aligned with axis q, axis β is 90 degree ahead of axis α in the counterclockwise direction and axis q is 90 degree ahead of axis d also in the counterclockwise direction yielding

$$\begin{bmatrix} i_d(t) \\ i_q(t) \\ i_0(t) \end{bmatrix} = T_1 \begin{bmatrix} i_\alpha(t) \\ i_\beta(t) \\ i_0(t) \end{bmatrix} = \begin{bmatrix} \cos(\omega t) & \sin(\omega t) & 0 \\ -\sin(\omega t) & \cos(\omega t) & 0 \\ 0 & 0 & 1 \end{bmatrix} \begin{bmatrix} i_\alpha(t) \\ i_\beta(t) \\ i_0(t) \end{bmatrix} \quad (2\text{-}32)$$

Combining equations (2-31) and equation (2-32) [22] yields

$$\begin{bmatrix} i_d(t) \\ i_q(t) \\ i_0(t) \end{bmatrix} = T_2 \begin{bmatrix} i_a(t) \\ i_b(t) \\ i_c(t) \end{bmatrix} = \begin{bmatrix} \cos(\omega t) & \sin\left(\omega t - \frac{2\pi}{3}\right) & \cos\left(\omega t + \frac{2\pi}{3}\right) \\ -\sin(\omega t) & -\sin\left(\omega t - \frac{2\pi}{3}\right) & -\sin\left(\omega t + \frac{2\pi}{3}\right) \\ \frac{1}{2} & \frac{1}{2} & \frac{1}{2} \end{bmatrix} \begin{bmatrix} i_a(t) \\ i_b(t) \\ i_c(t) \end{bmatrix} \quad (2\text{-}33)$$

Combining equations (2-4) - (2-10) , yields the switching function mathematical model of three-phase VSR in the three-phase static symmetric coordinate system as below:

$$\begin{cases} C\dfrac{dv_{dc}}{dt} = \sum\limits_{k\in\{a,b,c\}} i_k s_k - i_L \\ L\dfrac{di_k}{dt} + Ri_k = e_k - v_{dc}\left(s_k - \dfrac{1}{3}\sum\limits_{j\in\{a,b,c\}} s_j\right) \left(k \in \{a,b,c\}\right) \\ \sum\limits_{k\in\{a,b,c\}} e_k = \sum\limits_{k\in\{a,b,c\}} i_k = 0 \end{cases} \quad (2\text{-}34)$$

where, s_k —— unipolar boolean switch function ($k \in \{a, b, c\}$)

i_L —— VSR load current on the DC side

A block diagram implementation can be represented as the following:

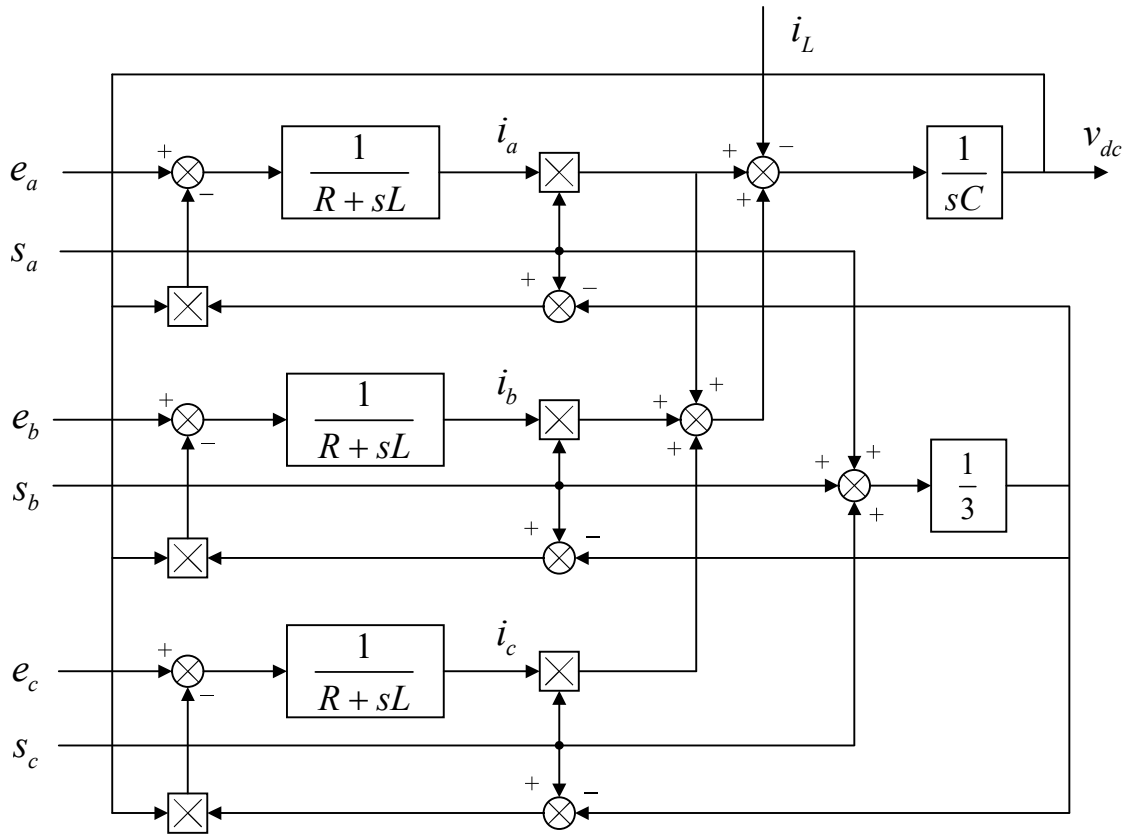

Figure 2.11 The switching function mathematical model of three-phase VSR in three-phase static symmetric coordinate system (a, b, c) [23]

In equation (2-33) , we used $i(t)$ as an example. We transformed $[i_a(t)\ i_b(t)\ i_c(t)]^T$ to $[i_d(t)\ i_q(t)\ i_0(t)]^T$. Generally we can apply the same transformation matrix T_2 to $[e_a(t)\ e_b(t)\ e_c(t)]^T$ and $[s_a(t)\ s_b(t)\ s_c(t)]^T$. Therefore, we get the mathematical model of the three-phase VSR in two-phase synchronously rotating coordinate system (d,q) as in equation (2-35) [23]:

$$\begin{cases} C\dfrac{dv_{dc}}{dt} = \dfrac{3}{2}\left(i_q s_q + i_d s_d\right) - i_L \\ L\dfrac{di_q}{dt} + \omega L i_d + R i_q = e_q - v_{dc} s_q \\ L\dfrac{di_q}{dt} - \omega L i_q + R i_d = e_d - v_{dc} s_d \end{cases} \tag{2-35}$$

The block diagram implementation can be represented as the following:

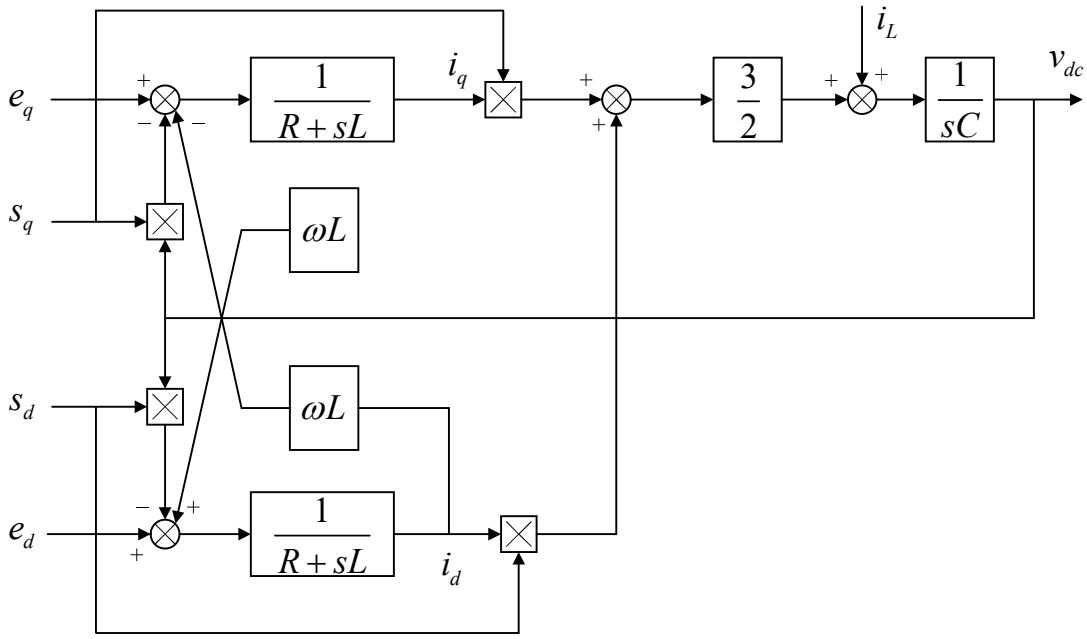

Figure 2.12 Model structure of three-phase VSR in two-phase synchronously rotating coordinate system (d, q)[23]

Chapter 3 Control of Three-phase VSR

3.1 Hysteresis Control

The main idea behind hysteresis control is using the output of a hysteresis function to drive the switching hardware. In our case, the difference between the setting current and the real current is the input to the hysteresis function and the result of comparing the difference with the threshold of the hysteresis yields an output which is the signal driving the power switches. The model structure is shown as in Figure 3.1.

First of all, we use Δv_{dc} , which is the difference between the setting output voltage on the DC side v_{dc}^{*} and real output voltage on the DC side v_{dc}, as the amplitude of the setting three-phase current. Then we multiply the amplitude by $\sin(\omega t+2k\pi/3)$ $(k \in \{0,1,2\})$ which synchronizes current on the AC side with voltage on the AC side yielding setting currents i^{*}_{a}, i^{*}_{b}, i^{*}_{c}. Next, we use the difference between setting current and real current Δi_k $(k \in \{a,b,c\})$ as the input of the hysteresis function. The result of comparing Δi_k with the threshold of the hysteresis is used to control the power switches. This way, the real current will be changing around the setting current. The less the difference, the more sinusoidal the real current becomes. Therefore we can achieve unity power factor.

The threshold has an impact on the characteristic of the hysteresis controller. A lower threshold yields a lower tracking error for the controller. However, there will be a higher

switching frequency leading to more switching loss. In contrast, less switching frequency, less switching loss. So, there is a tradeoff when choosing the appropriate threshold of the hysteresis in this method.

Hysteresis control can track the setting current effectively and therefore has a good robustness. Other advantages are the simplicity of model and quick response of current. Nevertheless, because the power switching frequency is not constant, this increases the design difficulty and impact to the system.

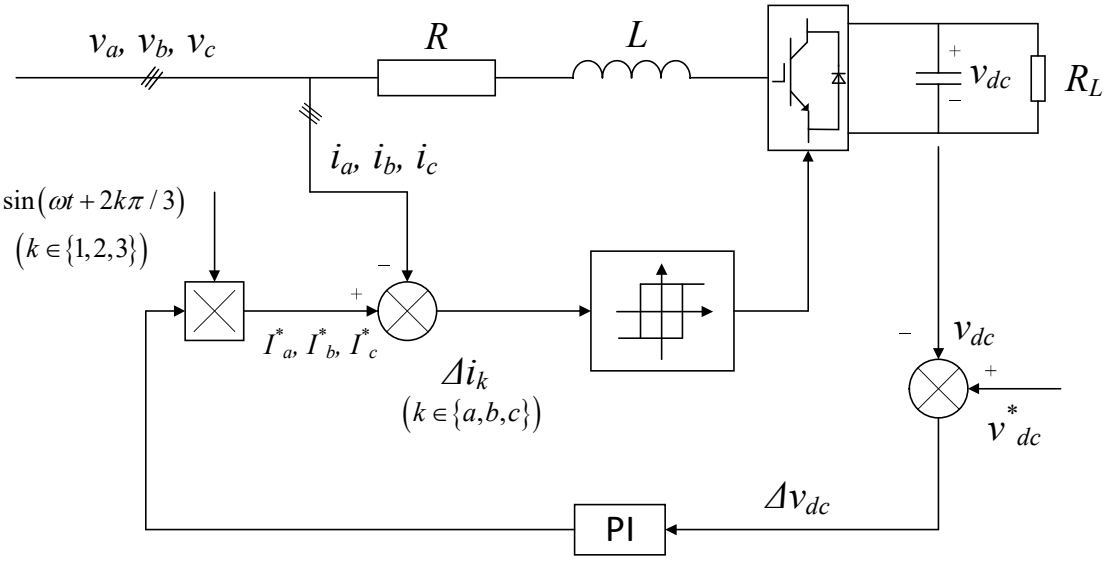

Figure 3.1 Model Structure of Hysteresis Control[24]

3.2 Double-loop decoupling SPWM control

The main idea in Double-loop decoupling SPWM control is using the difference of the setting current and the real current as the modulation wave to be compared with the

carrier wave having a constant frequency, and using the comparison result to control the power switches. The structure of the model is as in Figure 3.2.

There are two closed loops in the model, the voltage outer loop and the current inner loop. The parameter Δv_{dc} , the difference of the setting output voltage on the DC side v_{dc}^{*} and the real output voltage on DC v_{dc} is the input of the PI controller. The output of the PI controller is the amplitude of the active current setting current i^{*}_{d}. In our case reactive setting current i^{*}_{q} is 0. Through coordinate system transformation, we get the real current in two-phase synchronously rotating coordinate system (d,q) i_d representing the active current component, and i_q representing the reactive current component. Then we obtain the difference of setting current and real current. After decoupling and backward coordinate system transformation next we use the outcome as the modulation wave to be compared with the triangle carrier wave. Through some comparison logic we get the signal to control the power switches. Because the switching frequency is constant, we can constrain the switching loss and noise to some maximum level. Nevertheless, it is complicated to realize the control logic and the error in current tracking brings issues in the system.

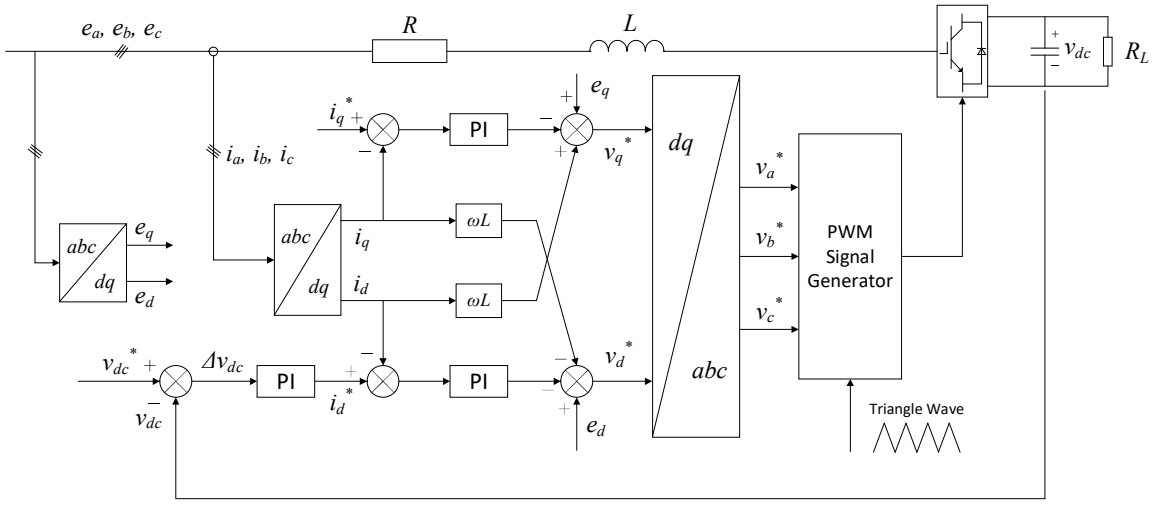

Figure 3.2 Double-loop decoupling control [25]

3.3 Double-loop decoupling SVPWM control

The main difference of Double-loop decoupling SVPWM control from Double-loop decoupling SPWM control is after we get v_d^* and v_q^*, we do not feed them into PWM Signal Generator anymore. Instead we feed them into a SVPWM (Space Vector PWM) Signal Generator. T_s here refers to the period of the triangle carrier wave. The structure of the model is as in Figure 3.3. We will discuss the details inside the module SVPWM Signal Generator in the next subsection.

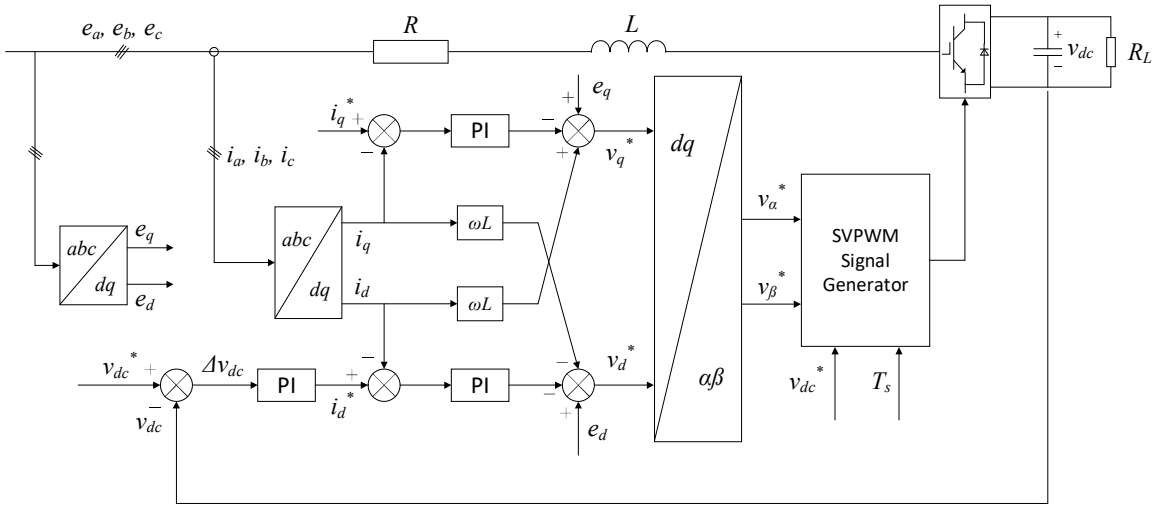

Figure 3.3 The Model Structure of SVPWM Control

3.3.1 Principle of SVPWM Modulation

From the quasi-circle magnetic flux in AC asynchronous motor control theory, the novel Space Vector Control method is broadly adopted in three-phase three bridge arms without neutral line converting system[26].

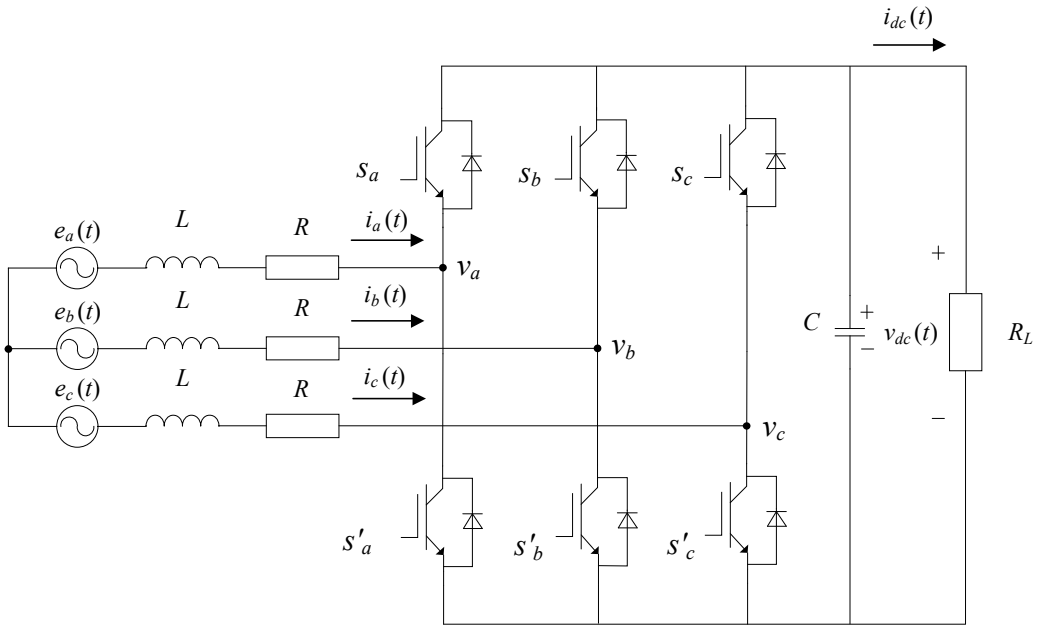

Figure 3.4 A Typical Model of Three-phase Converting System

Figure 3.4 shows a typical model of three-phase converting system, where, v_a, v_b, v_c are the output phase voltage. We define v_{ab}, v_{bc}, v_{ca} as the phase-to-phase voltage as follows.

$$v_{ab} = v_a - v_b \tag{3-1}$$

$$v_{bc} = v_b - v_c \tag{3-2}$$

$$v_{ca} = v_c - v_a \tag{3-3}$$

$$v_{kO} = v_{kN} + v_{NO} = v_{dc} s_k + v_{NO} \qquad \left(k \in \{a,b,c\}\right) \tag{3-4}$$

Combining equations (2-8) , (3-1) ~ (3-4) yields

$$\begin{bmatrix} v_a \\ v_b \\ v_c \end{bmatrix} = \frac{1}{3} v_{dc} \begin{bmatrix} 2 & -1 & -1 \\ -1 & 2 & -1 \\ -1 & -1 & 2 \end{bmatrix} \begin{bmatrix} s_a \\ s_b \\ s_c \end{bmatrix} \tag{3-5}$$

$$\begin{bmatrix} v_{ab} \\ v_{bc} \\ v_{ca} \end{bmatrix} = v_{dc} \begin{bmatrix} 1 & -1 & 0 \\ 0 & 0 & 1 \\ -1 & 0 & 1 \end{bmatrix} \begin{bmatrix} s_a \\ s_b \\ s_c \end{bmatrix} \tag{3-6}$$

As mentioned earlier in chapter 2, there are eight combinations in total in switching. The corresponding phase-to-ground voltage and phase-to-phase voltage in different switching combinations are shown in Table 3-1.

Table 3-1 Corresponding phase-to-ground voltages and phase-to-phase voltages in different switching combinations

s_a	s_b	s_c	v_a	v_b	v_c	v_{ab}	v_{bc}	v_{ca}
0	0	0	0	0	0	0	0	0
1	0	0	$2v_{dc}/3$	$-v_{dc}/3$	$-v_{dc}/3$	v_{dc}	0	$-v_{dc}$
0	1	0	$-v_{dc}/3$	$2v_{dc}/3$	$-v_{dc}/3$	$-v_{dc}$	v_{dc}	0
1	1	0	$v_{dc}/3$	$v_{dc}/3$	$-2v_{dc}/3$	0	v_{dc}	$-v_{dc}$
0	0	1	$-v_{dc}/3$	$-v_{dc}/3$	$2v_{dc}/3$	0	$-v_{dc}$	v_{dc}
1	0	1	$v_{dc}/3$	$-2v_{dc}/3$	$v_{dc}/3$	v_{dc}	$-v_{dc}$	0
1	1	0	$v_{dc}/3$	$v_{dc}/3$	$-2v_{dc}/3$	$-v_{dc}$	0	v_{dc}
1	1	1	0	0	0	0	0	0

If we map the switching combinations to vectors with norm being $2v_{dc}/3$, we can easily represent all 8 combinations in a complex plane. The 6 vectors (from v_0 to v_{300})

divide the plane into 6 sectors evenly, where v_{000} and v_{111} are called zero vectors since they have a norm of zero.

Every switching combination corresponds to a space vector, if we project the space vector to (a, b, c) coordinate system, we attain the corresponding phase voltages.

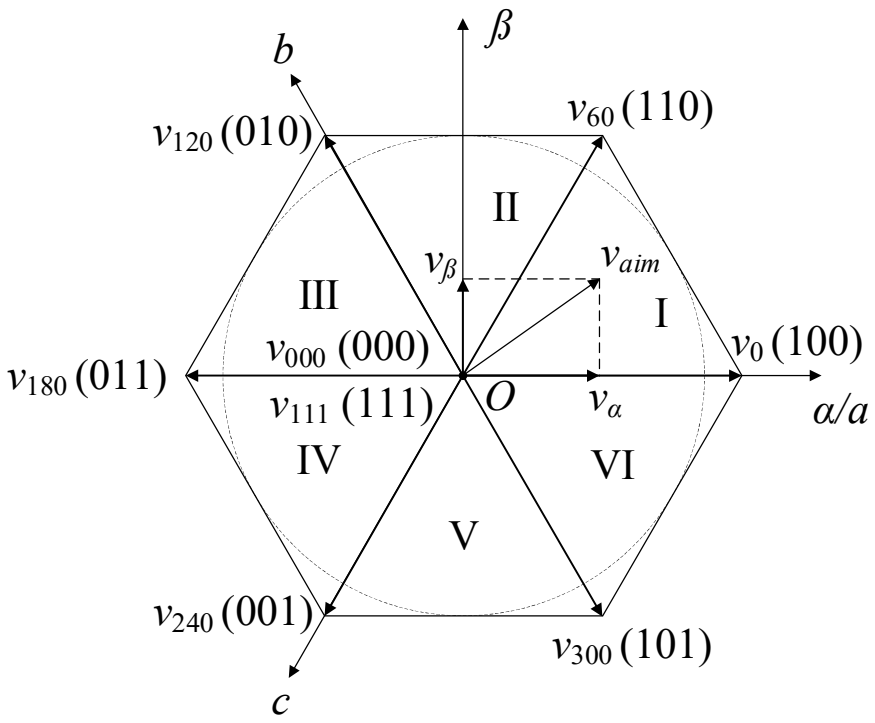

Figure 3.5 Distribution of Voltage Vector Space[26]

Here we define the voltage space vector v_{ref} as:

$$v_{ref} = \frac{2}{3}\left(v_a + v_b e^{j2\pi/3} + v_c e^{j4\pi/3}\right) = v_\alpha + jv_\beta \tag{3-7}$$

Where v_a, v_b, v_c are the norms of corresponding phase voltage when v_{ref} is projected to (a, b, c) coordinate system, and v_α, v_β are the norms of corresponding phase voltage when v_{ref} is projected to (α, β) coordinate system. Vector v_{ref} rotates at the speed of ω counterclockwise whose trajectory of vector endpoint is a quasi circle shown as dashed line in Figure 3.5.

v_{ref} in any of the six sectors can be composed by the two adjacent vectors based on voltage-second balance.

3.3.2 Realization of SVPWM Modulation

In order to obtain the two adjacent vectors, first we locate the reference vector so that we know the norm and phase angle of the vector based on which we can find out the time of switch-on time of the adjacent vectors and further, we can figure out the switching time by some logic. Two out of the six space vectors are zero vectors represented by v_{000} and v_{111}. The operating time of the zero vectors are the time left in a switching period after considering other vectors. Concerning the operating order of the vectors including zero vectors, we want the order such that the switching events occur infrequently to reduce the switching loss. In addition, we usually adopt a symmetric order for the operation of the vectors to attain a symmetric PWM signal to diminish the higher harmonics component in it.

To adopt the SVPWM, we need to transform our reference vector in three-phase static coordinate system to two-phase static coordinate system first. The transformation is as in equation (3-8).

$$\begin{bmatrix} v_\alpha \\ v_\beta \end{bmatrix} = \frac{2}{3}\begin{bmatrix} 1 & -\frac{1}{2} & -\frac{1}{2} \\ 0 & \frac{\sqrt{3}}{2} & -\frac{\sqrt{3}}{2} \end{bmatrix}\begin{bmatrix} v_a \\ v_b \\ v_c \end{bmatrix} \tag{3-8}$$

1. Nailing down the sector.

According to Figure 3.5, when v_{ref} is in sector I, we get:

$$0 < \arctan\left(\frac{v_\beta}{v_\alpha}\right) < \frac{\pi}{3} \tag{3-9}$$

In addition to the inequality above considering the geometric relationship in Figure 3.5, we can conclude that the necessary and sufficient condition of v_{ref} in sector I is:

$$v_\alpha > 0, v_\beta > 0 \text{ and } \frac{v_\beta}{v_\alpha} < \sqrt{3} \tag{3-10}$$

Similarly, we can get the necessary and sufficient conditions of v_{ref} in other sectors, so we form the table below:

Table 3-2 Necessary and Sufficient Conditions of v_{ref} in Sector N

Sector	Necessary and Sufficient Condition
I	$v_\alpha > 0, v_\beta > 0 \; and \; \frac{v_\beta}{v_\alpha} < \sqrt{3}$
II	$v_\beta > 0 \; and \; \frac{v_\beta}{\lvert v_\alpha \rvert} > \sqrt{3}$
III	$v_\alpha < 0, v_\beta > 0 \; and \; -\frac{v_\beta}{v_\alpha} < \sqrt{3}$
IV	$v_\alpha < 0, v_\beta > 0 \; and \; \frac{v_\beta}{v_\alpha} < \sqrt{3}$
V	$v_\beta > 0 \; and \; -\frac{v_\beta}{\lvert v_\alpha \rvert} > \sqrt{3}$
VI	$v_\alpha > 0, v_\beta < 0 \; and \; -\frac{v_\beta}{v_\alpha} < \sqrt{3}$

We can find out from the table above that we can locate the vector by judging whether the following expressions are greater than zero or not:

$$\begin{cases} v_\beta, \\ \sqrt{3}v_\alpha - v_\beta, \\ -\sqrt{3}v_\alpha - v_\beta \end{cases} \tag{3-11}$$

Here we define variables $A,\ B,\ C$. When $v_\beta > 0$, $A = 1$, otherwise, $A = 0$. When $\sqrt{3}v_\alpha - v_\beta > 0$, $B = 1$, otherwise, $B = 0$. When $-\sqrt{3}v_\alpha - v_\beta > 0$, $C = 1$, otherwise, $C = 0$. Different combinations of $A,\ B,\ C$ corresponds to different sectors, and there are six

combinations of $A,\ B,\ C$ whose corresponding vectors' norms are nonzero and the rest two. For convenience of judging the sectors, we define $N = A+2B+4C,$ so we obtain

the relationship between value of N and corresponding sectors as in Table 3-3.

Table 3-3 N and it corresponding sectors

Sector	I	II	III	IV	V	VI
N	3	1	5	4	6	2

2. Determining Vector Operation Time

We here analyze the case located at sector I as an example, according to Figure 3.5, we can attain:

$$\begin{cases} |v_0|T_0 + |v_{60}|T_{60}\cos 60^\circ = v_\alpha T_s \\ |v_{60}|T_{60}\sin 60^\circ = v_\beta T_s \end{cases} \tag{3-12}$$

where, T_s is sample period. Parameters T_0 and T_{60} are the operation time of voltage vectors v_0 and v_{60} during a sample period respectively. We can find:

$$\begin{cases} T_0 = \dfrac{T_s\left(3v_\alpha - \sqrt{3}v_\beta\right)}{2v_{dc}} \\ T_{60} = \dfrac{\sqrt{3}v_\beta T_s}{v_{dc}} \\ T_{000} = T_{111} = \dfrac{1}{2}\left(T_s - T_0 - T_{60}\right) \end{cases} \tag{3-13}$$

where T_{000} and T_{111} are the vector operation time of vectors v_{000} and v_{111}.

Similarly, we attain the operation time of the adjacent space vectors in rest of the sectors, and for convenience of expression purpose, we introduce intermediate variables X, Y, Z and define:

$$\begin{cases} X = \dfrac{\sqrt{3}v_\beta T_s}{v_{dc}} \\ Y = \dfrac{3}{2}\dfrac{v_\alpha T_s}{v_{dc}} + \dfrac{\sqrt{3}}{2}\dfrac{v_\beta T_s}{v_{dc}} \\ Z = -\dfrac{3}{2}\dfrac{v_\alpha T_s}{v_{dc}} + \dfrac{\sqrt{3}}{2}\dfrac{v_\beta T_s}{v_{dc}} \end{cases} \tag{3-14}$$

T_1 represents the operation time of the vector operating first in corresponding vector, T_2 represents the operation time of the vector operating second in corresponding vector, so we obtain the table of the operation time of two base vectors in corresponding vectors as in Table 3-4.

Table 3-4 Operation time of two base vectors in corresponding vectors

Sectors / Base vectors operation time	I	II	III	IV	V	VI
T_1	-Z	Z	X	-X	-Y	Y
T_2	X	Y	-Y	X	-X	-X

When $T_1 + T_2 > T_s$, we do a correction here as:

$$\begin{cases} T_1' = \dfrac{T_1}{T_1 + T_2} \times T_s \\ T_2' = \dfrac{T_2}{T_1 + T_2} \times T_s \end{cases} \tag{3-15}$$

3. Nailing down the vector switching points

As mentioned earlier in this chapter, we can attain the aim voltage vector by composing it with two adjacent vectors as base vectors and choose an appropriate operation time of them to get the desired proportion out of the base vector. Here, we compose an aim voltage vector in sector I as an example in Figure 3.6, and its corresponding switching function as in Figure 3.7.

We sever the aim voltage vector in the middle by putting a zero vector v_{111} there with operation time T_{111} and we put the other zero vector v_{000} to both the beginning and end with equal operation time $T_{000} / 2$. We make the switching function symmetric which can reduce the PWM higher harmonics[27].

According to the method mentioned above, we obtain:

$$\begin{cases} t_{on\,a} = \dfrac{T_s - T_1 - T_2}{4} \\ t_{on\,b} = t_{on\,a} + \dfrac{T_1}{2} \\ t_{on\,c} = t_{on\,b} + \dfrac{T_2}{2} \end{cases} \tag{3-16}$$

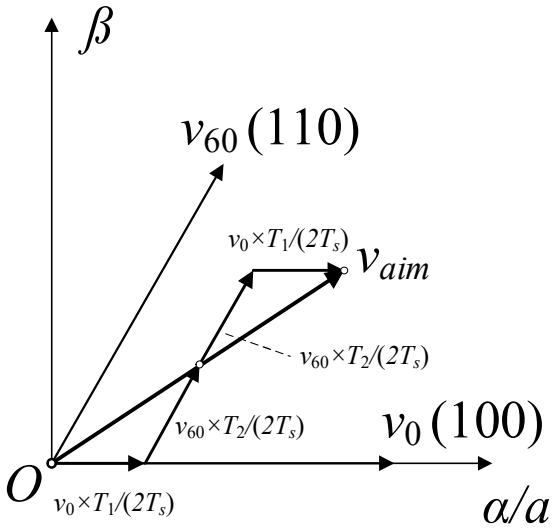

Figure 3.6 Vector Composition in Sector I

Similarly, we can attain the switching time on other sectors as in:

Table 3-5 Switching time in sectors

N / Switching Time	1	2	3	4	5	6
t_{on1}	$t_{on\,b}$	$t_{on\,a}$	$t_{on\,a}$	$t_{on\,c}$	$t_{on\,c}$	$t_{on\,b}$

t_{on2}	$t_{on\ a}$	$t_{on\ c}$	$t_{on\ b}$	$t_{on\ b}$	$t_{on\ a}$	$t_{on\ c}$
t_{on3}	$t_{on\ c}$	$t_{on\ b}$	$t_{on\ c}$	$t_{on\ a}$	$t_{on\ b}$	$t_{on\ a}$

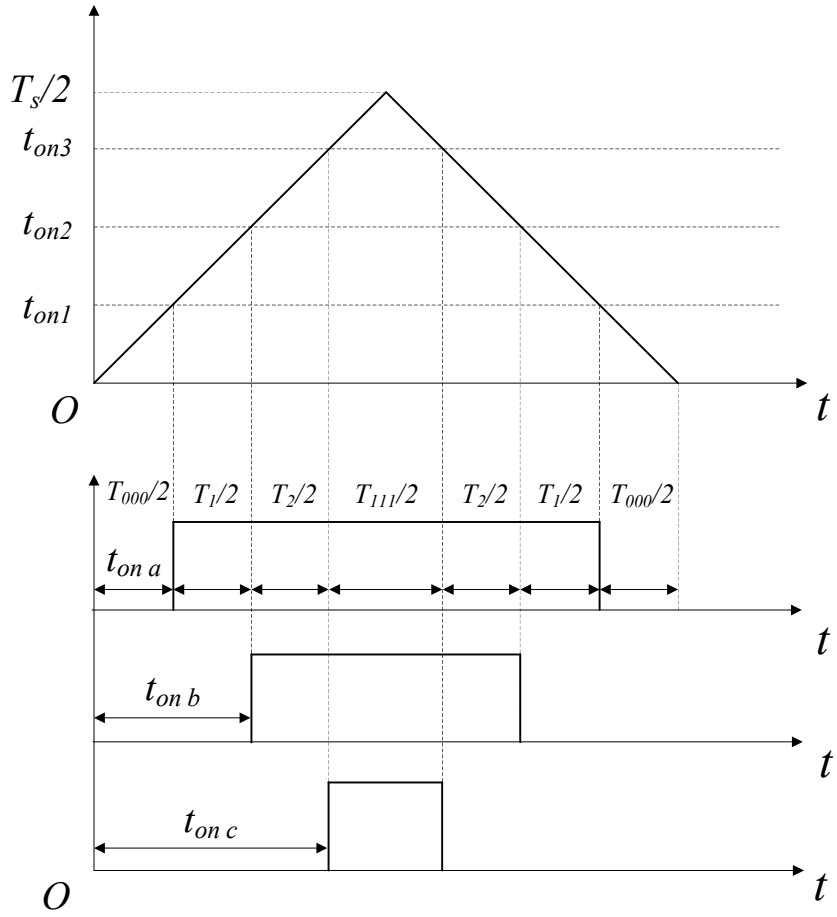

Figure 3.7 Corresponding Switching Function of Vector in Sector I

We compare the switching time with a triangle carrier wave similarly in Figure 3.7 to get the PWM signals to drive switches.

Chapter 4 Simulation

To verify the theories, control methods and do comparison on power loss in switching among three control methods mentioned in previous chapters, I built the models in MATLAB / Simulink.

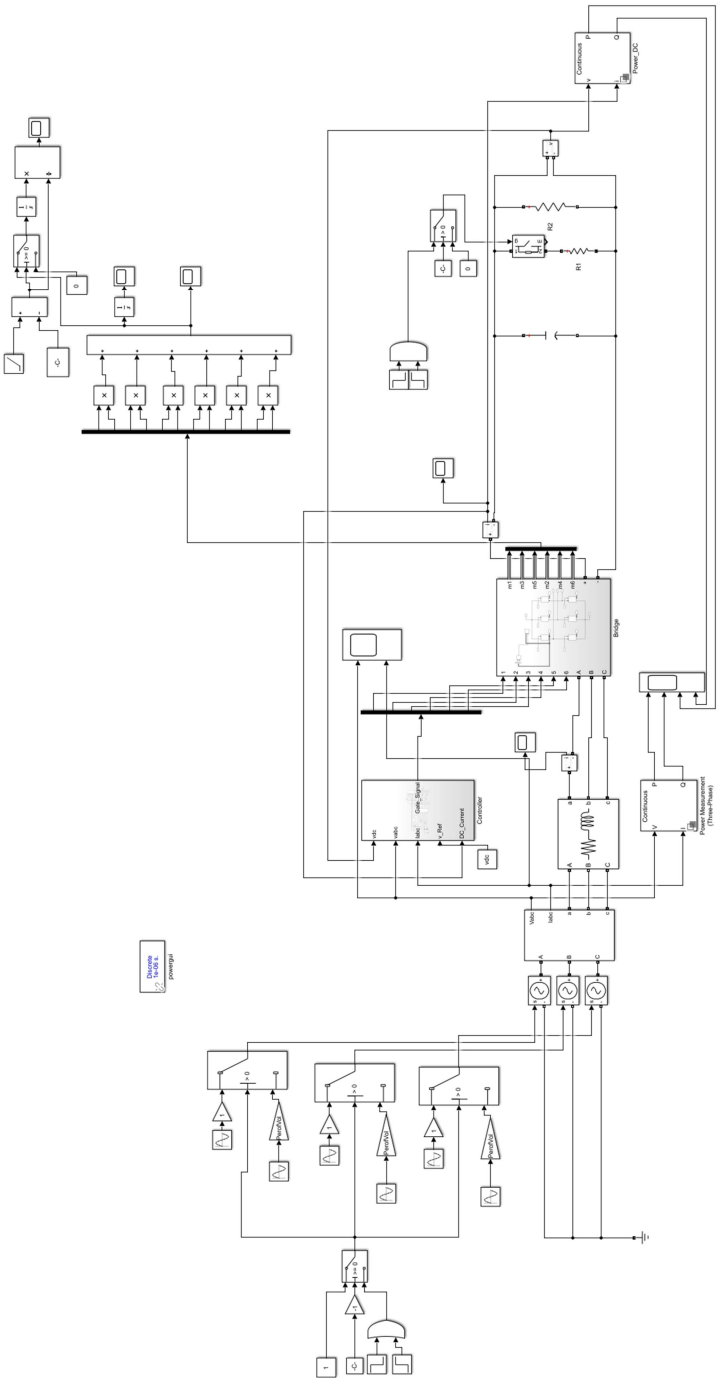

Figure 4.1 Simulation of Three-phase rectifier system

4.1 System Model and Parameters

As in Figure 4.1, a MATLAB / Simulink model is built. Three controlled voltage sources are used to simulate three-phase balanced voltage source. Their input signals are three sine waves with frequency of 60 Hz, with RMS value of the AC side phase voltage 120 V and, phases of 0, -2/3*pi and -4/3*pi respectively. The AC side input filter inductance is 20 mH. The AC side equivalent resistance is 0.2 ohms. The DC side load R1 is 200 ohms and R2 is 100 ohms. The DC side filter capacitor is 680 µF. Carrier wave frequency is 1e4 Hz. Six MOSFETs are used in the three-phase half bridge. The switch MOSFET is from Simscape / Electrical / Specialized Power Systems / Fundamental Blocks / Power Electronics in Simulink Browser. The settings and parameters of the MOSFETs are as in Figure 4.2. Solver ode45 is adopted in the simulation.

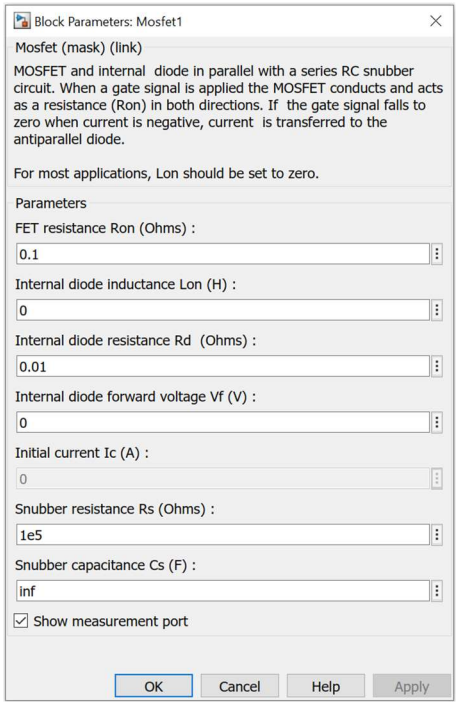

Figure 4.2 Setting and Parameters of MOSFET

The main modules in the simulation are: three-phase balanced grid, AC filter inductor, three-phase half bridge arms, and controller module. Three different control methods are adopted which are inside the controller module. I am going to show the logic and subsystems inside the controller module in detail later in this chapter.

4.1.1 Determining the DC side voltage

There are two main aspects worth considering in determining the voltage level of the DC side voltage. On one hand, the voltage should be high enough to meet the power requirement of the load and obtain the expected current wave on the AC side. On the other hand, the higher the voltage level, the more stringent requirement on the materials

to withstand high voltage of components on the DC side which means higher cost. So, there is a trade-off here.

Also, there are restrictions in both three-phase double-loop decoupling SPWM method and three-phase double-loop decoupling SVPWM method. Inequalities (4-1) and (4-2) [28] show the corresponding restrictions in SPWM and SVPWM respectively.

$$v_{dc} \geq 2 \times \sqrt{2} \times v_s \tag{4-1}$$

$$v_{dc} \geq \sqrt{3} \times \sqrt{2} \times v_s \tag{4-2}$$

where v_{dc} is the DC side voltage, v_s is root mean square phase voltage on the AC side. In the simulation $|v_s| = 120\,\mathrm{V}$. $v_{dc} \geq 339.41\,\mathrm{V}$. We assign $v_{dc} = 360\,\mathrm{V}$ in the simulation.

4.1.2 Determining capacitance of the DC side filter capacitor

The filter capacitor on the DC side can smooth the output DC voltage, reduce the ripple in output voltage and help enhance the robustness of system by decreasing the rate of change of the output voltage when the load changes. The greater the capacitance, the better the function of the capacitor mentioned above will be. On the other hand, if the capacitance gets too large, it begins to degrade the dynamics of the DC side voltage tracking the setting voltage. So, there is a trade-off between the two different considerations.

Taking the two the aspects into account, we can get a range of the capacitance by equation (4-3) [29]:

$$\frac{1}{2\Delta v_{dc} R_L} < C < \frac{t_r}{0.74 R_L} \tag{4-3}$$

where Δv_{dc} is the error of the DC side voltage, R_L is the DC side load, t_r is the rising time of the DC side voltage. Here we let $\Delta v_{dc} = 36\,\mathrm{V}$, $R_L = 100\,\Omega$ and $t_r = 0.1\,\mathrm{s}$. So, we obtain the reference range of the capacitance:

$$138.89\,\mu\mathrm{F} < C < 1400\,\mu\mathrm{F} \tag{4-4}$$

In the simulation we assign $C = 680\,\mu\mathrm{F}$.

4.1.3 Determining inductance of the AC side filter inductor

There are two aspects worth considering in determining the inductance of the AC side filter inductor. On one hand, the larger the inductance, the less ripple there will be in AC input current. On the other hand, the less inductance, the better dynamic performance and the lower cost. So, taking the two aspects into account, we can get a range of the inductance value in (4-5) [29]:

$$\frac{15v_s}{P}\left(\frac{\sqrt{2}v_s\omega T_s^2}{4}+\frac{v_{dc}}{3}T_s\right)\le L\le\frac{0.9v_s^2}{P\omega} \tag{4-5}$$

where, v_s is the AC side RMS phase voltage, $v_s=120\,\mathrm{V}$, P is the power level of the system, $P=v_{dc}^2/R_L$, E_m is the RMS value of the phase electromotive force on the AC side, ignoring the resistance and inductance on the AC side, so $E_m=v_s$. ω is the angular frequency of the power supply. T_s is the period of PWM carrier wave. Plugging the variables into the inequality, we attain the range:

$$16.9\ \mathrm{mH}\le L\le 26.5\ \mathrm{mH} \tag{4-6}$$

We pick up 20 mH as the inductance.

4.1.4 Controller Module

1. Hysteresis method

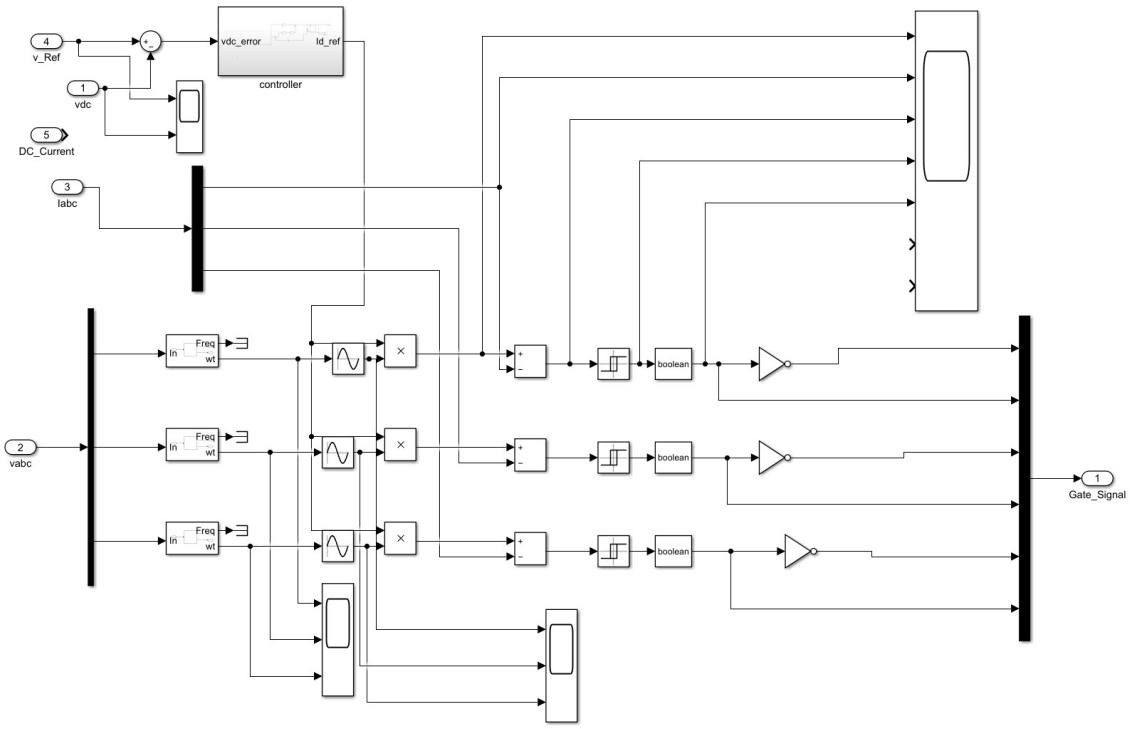

Figure 4.3 Control Module of Hysteresis Control Method

The module shown in Figure 4.3 is built based on the model structure in Figure 3.1. The setting of the relay module is shown in Figure 4.4.

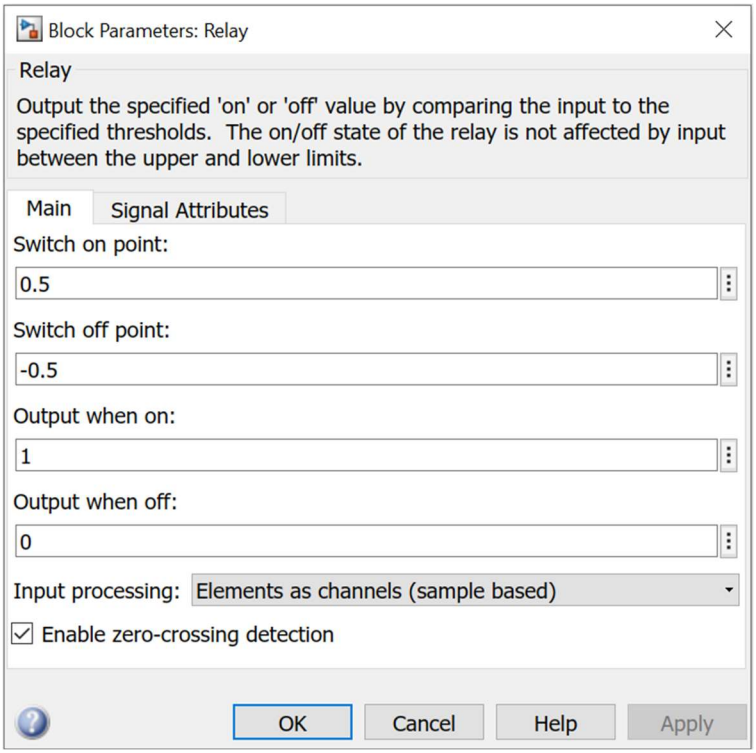

Figure 4.4 Setting of Relay Module

Figure 4.5 shows the hysteresis function input for the AC side phase a current, the upper bound and the lower bound of the hysteresis function are 0.5 and -0.5, as shown in the picture, the input is regulated between the bounds. Figure 4.6 is the zooming in of Figure 4.5.

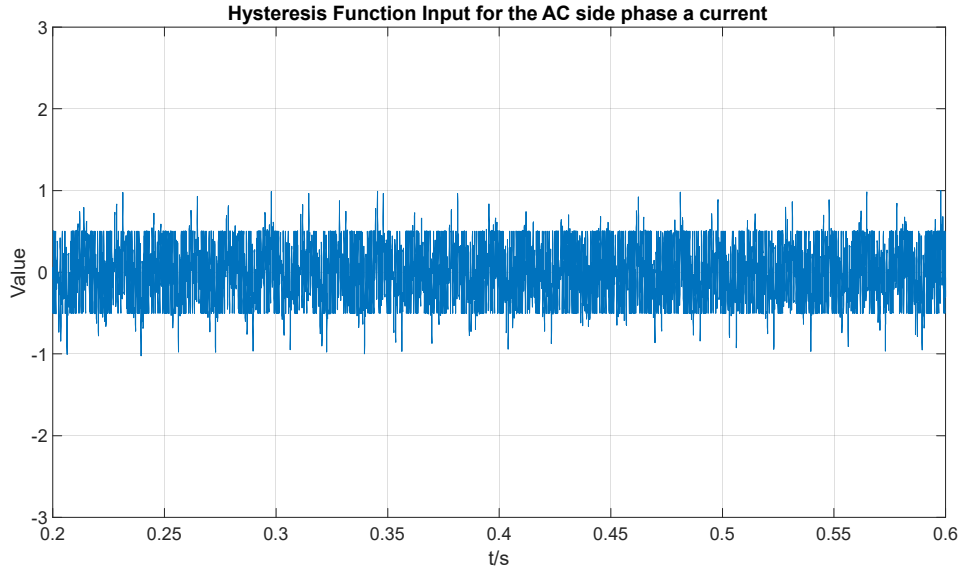

Figure 4.5 Hysteresis Function Input for the AC Side Phase a Current

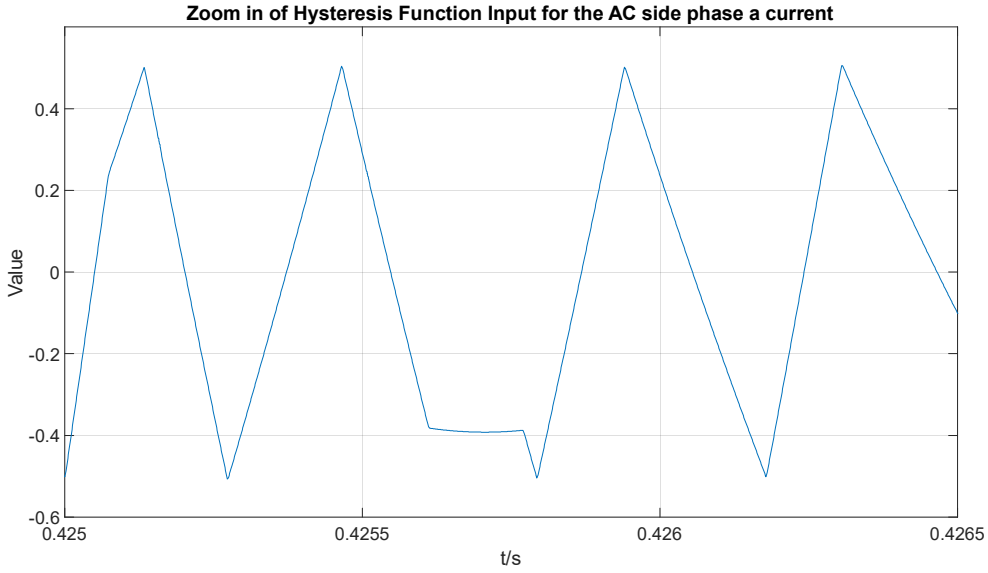

Figure 4.6 Zoom in of Hysteresis Function Input for the AC Side Phase a Current

Figure 4.7 shows the bode diagram of PI controller of the voltage loop in hysteresis method.

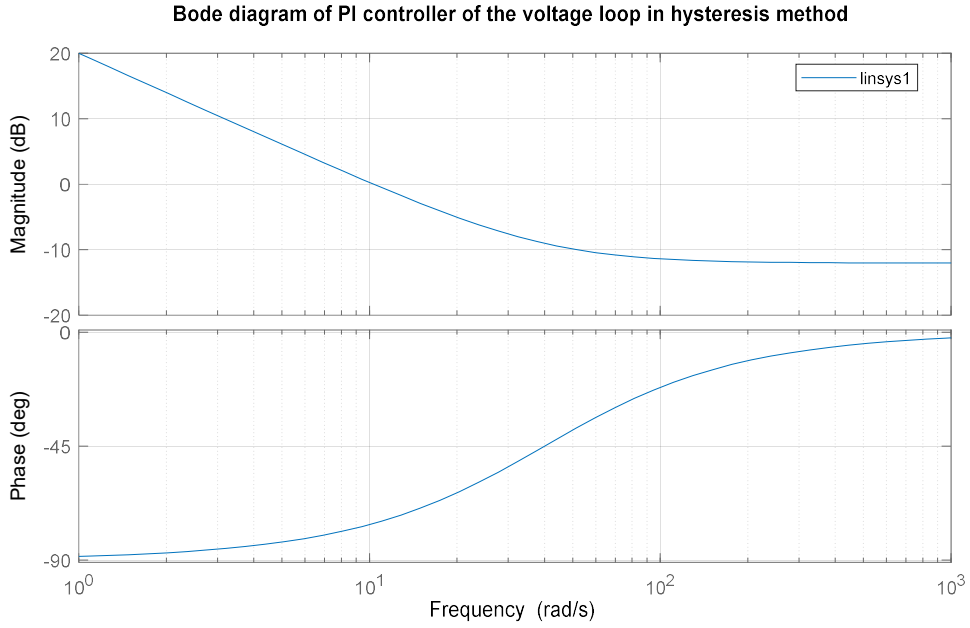

Figure 4.7 The bode diagram of PI controller of the voltage loop in hysteresis method

2. Double-loop decoupling SPWM control method

The control module of double-loop decoupling control method in Figure 4.8 is built based on the logics and model structure in Figure 3.2.

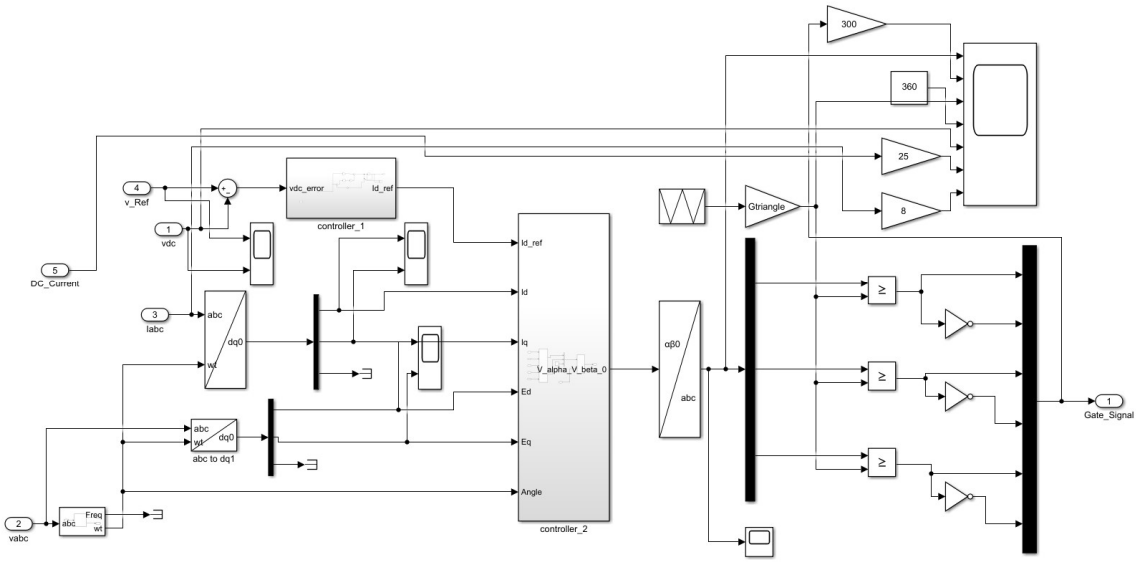

Figure 4.8 Control module of Double-loop decoupling SPWM control method

Figure 4.9 - Figure 4.11 show bode diagram of PI controllers in double-loop decoupling SPWM method.

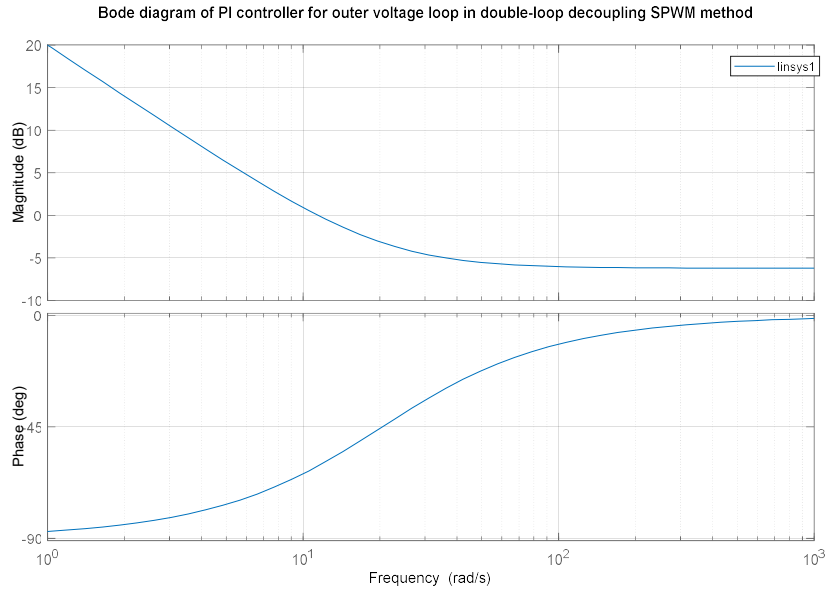

Figure 4.9 Bode diagram of PI controller for outer voltage loop in double-loop decoupling SPWM method

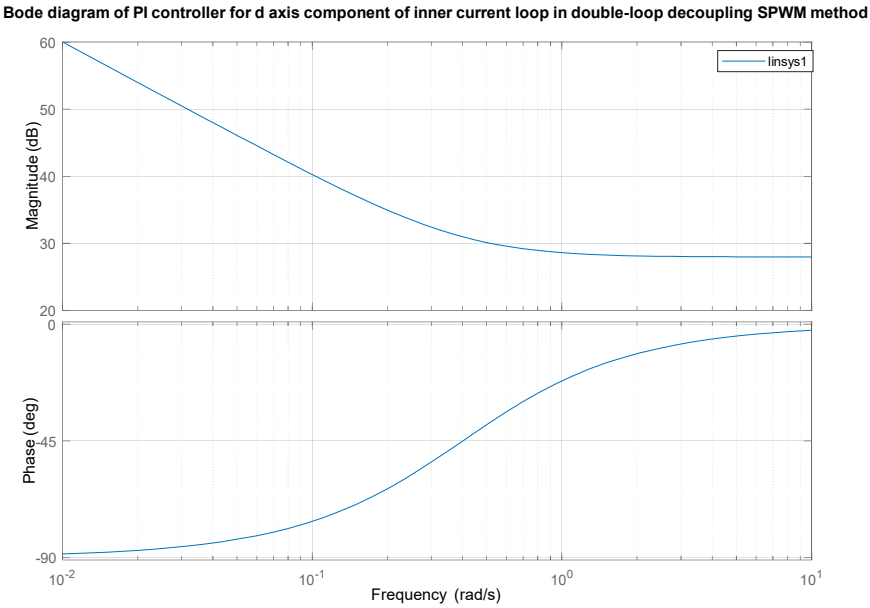

Figure 4.10 Bode diagram of PI controller for d axis component of inner current loop in double-loop decoupling SPWM method

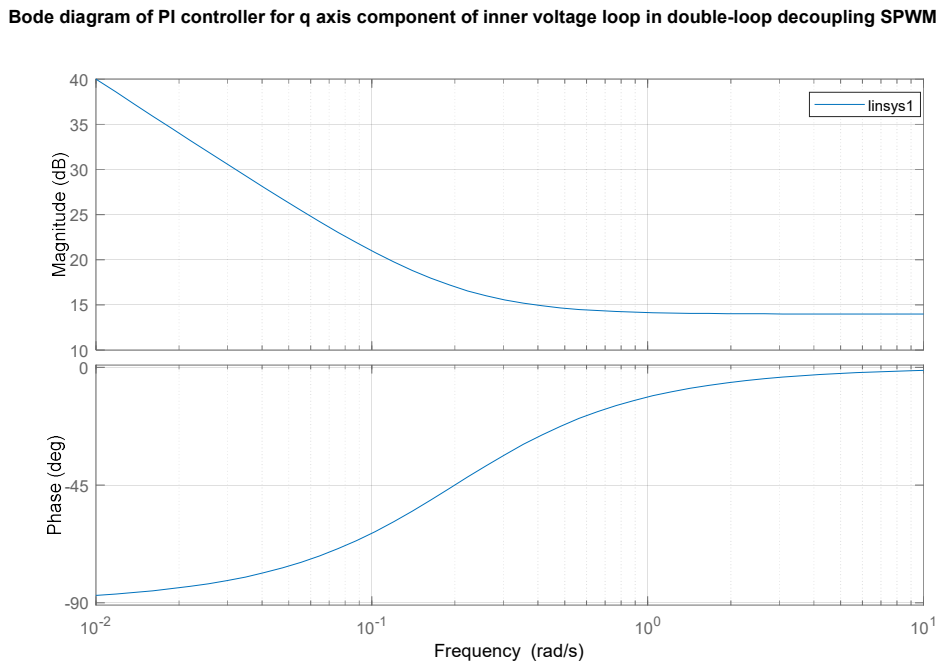

Figure 4.11 Bode diagram of PI controller for q axis component of inner current loop in double-loop decoupling SPWM method

Figure 4.12 - Figure 4.14 show bode diagram of PI controllers in double-loop decoupling SVPWM method.

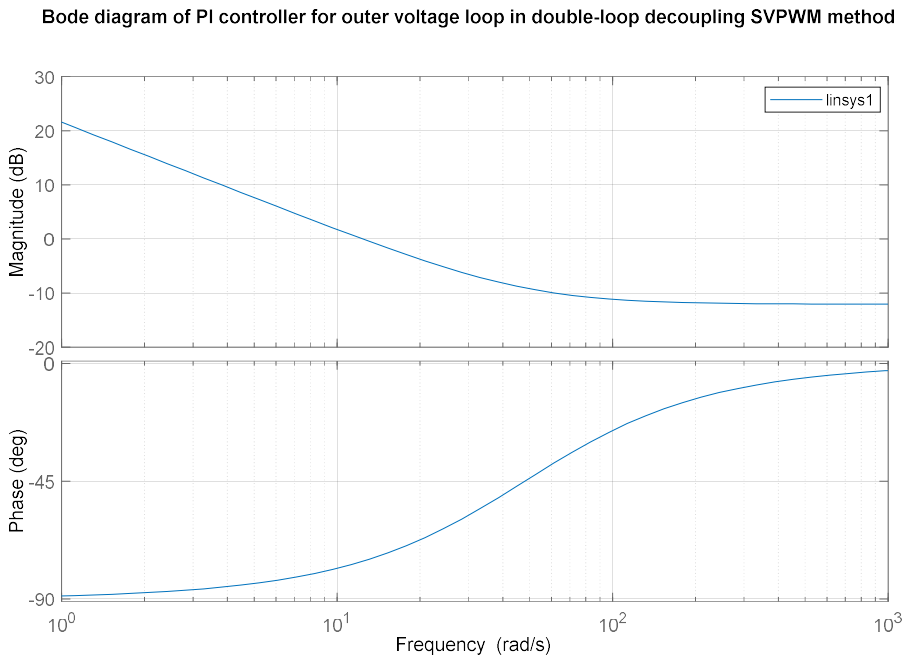

Figure 4.12 Bode diagram of PI controller for outer voltage loop in double-loop decoupling SVPWM method

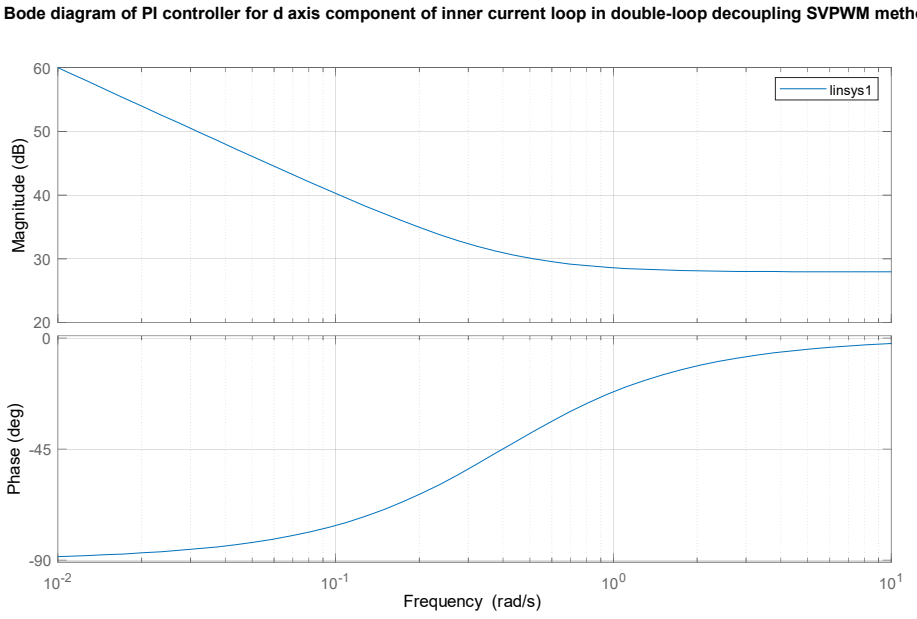

Figure 4.13 Bode diagram of PI controller for d axis component of inner current loop in double-loop decoupling SVPWM method

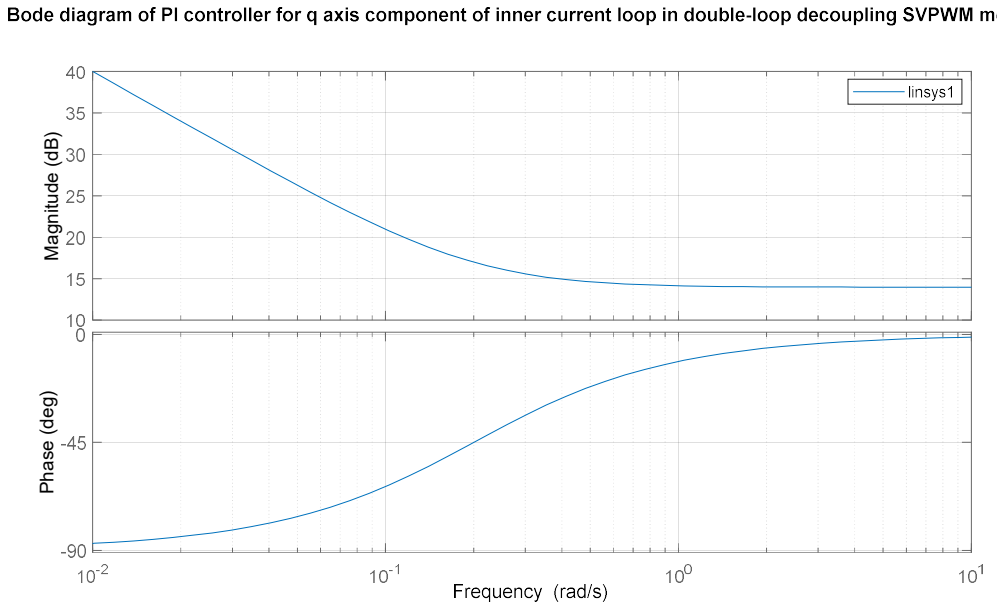

Figure 4.14 Bode diagram of PI controller for q axis component of inner current loop in double-loop decoupling SVPWM method

3. Double-loop decoupling SVPWM control method

The control module of double-loop decoupling SVPWM control method in Figure 4.15 is built based on the logic and model structure in Figure 3.3.

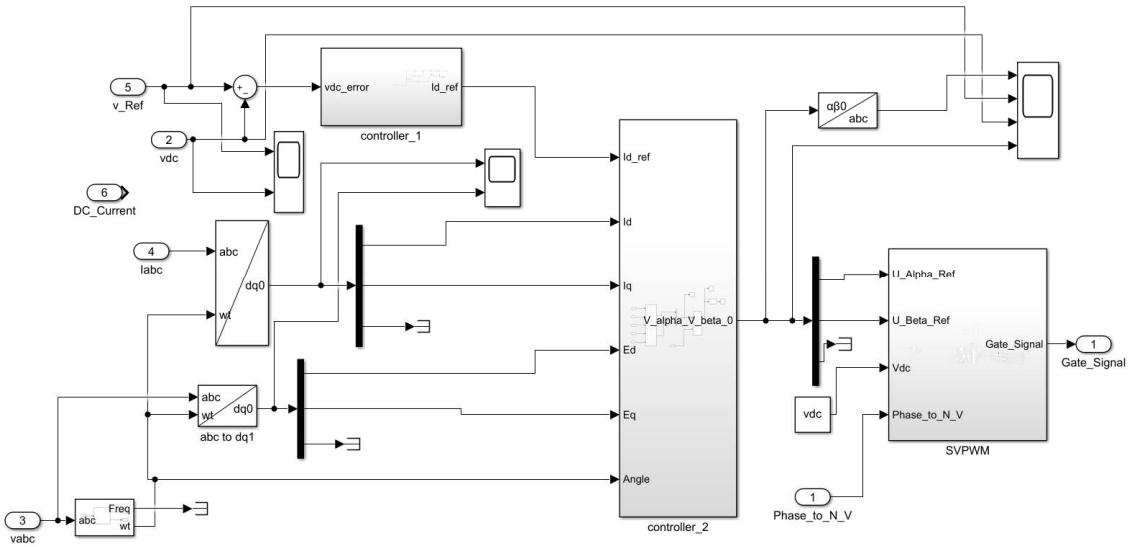

Figure 4.15 Control module of Double-loop decoupling SVPWM control method

4.1.5 SVPWM Module

There are several main subsystems inside SVPWM module in Figure 4.15 which are sector judge subsystem, intermediate variables generator subsystem, adjacent vectors operation time calculator subsystem and switching time calculator subsystem. On the bottom right corner of the SVPWM module is the PWM signal generating section. The SVPWM module is shown in Figure 4.16.

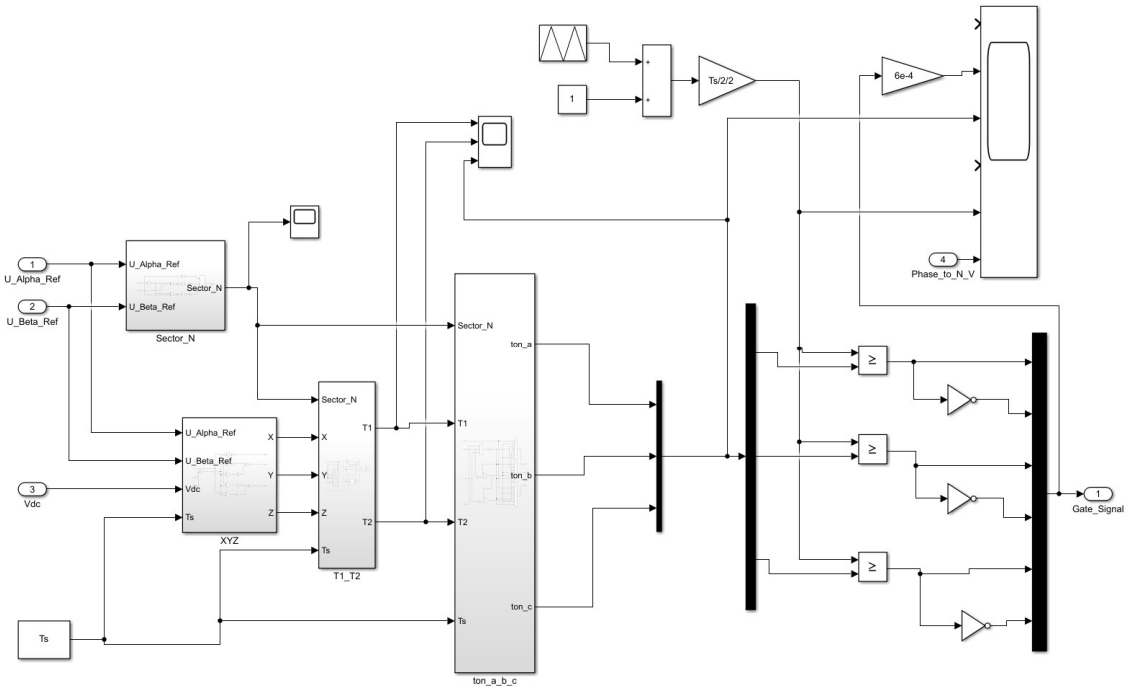

Figure 4.16 SVPWM module

1. Sector Judge Subsystem

Figure 4.17 shows the sector judge subsystem.

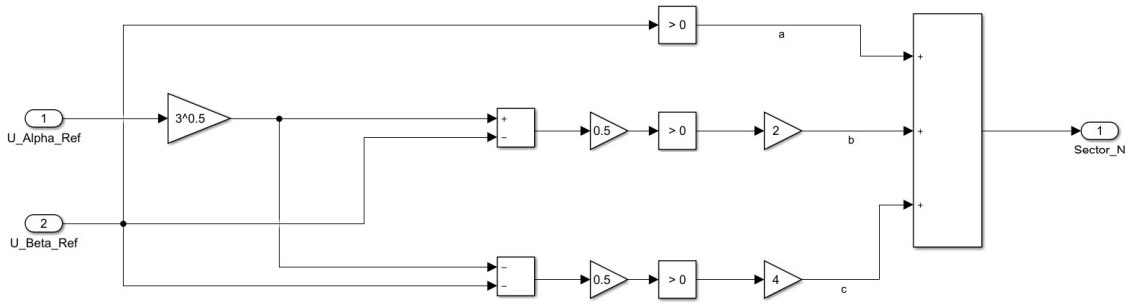

Figure 4.17 Sector Judge Subsystem

2. Intermediate Variables Generator

Figure 4.18 shows the intermediate variables generator subsystem.

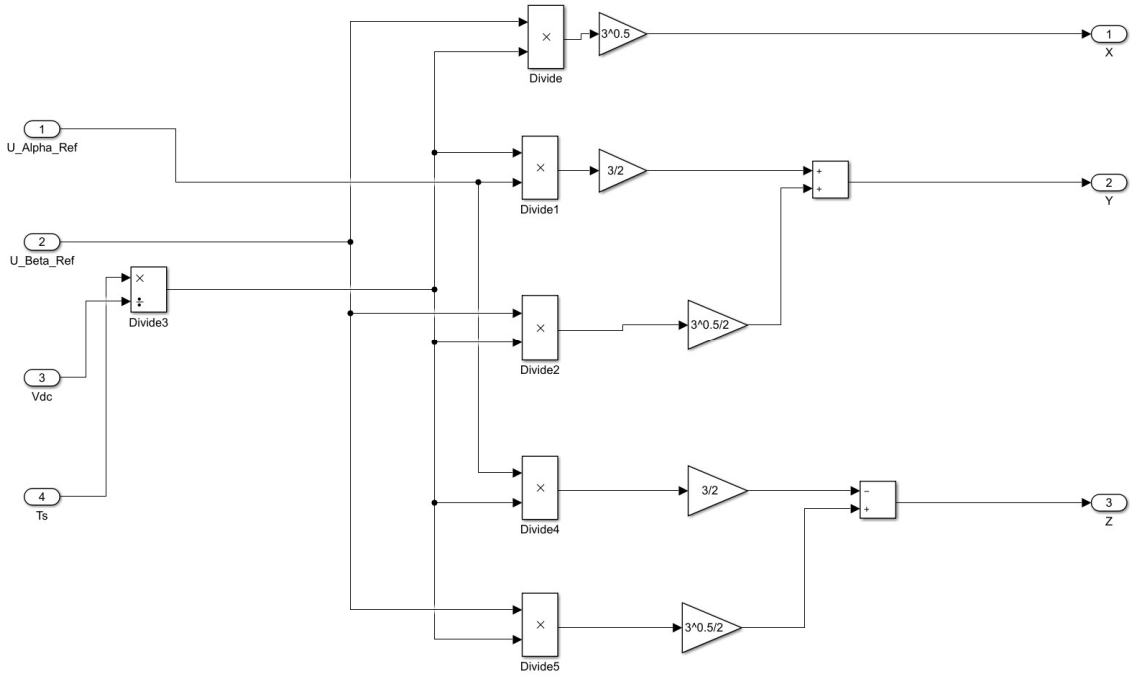

Figure 4.18 Intermediate variables generator subsystem

3. Adjacent vectors operation time calculator subsystem

Figure 4.19 shows adjacent vectors operation time calculator subsystem.

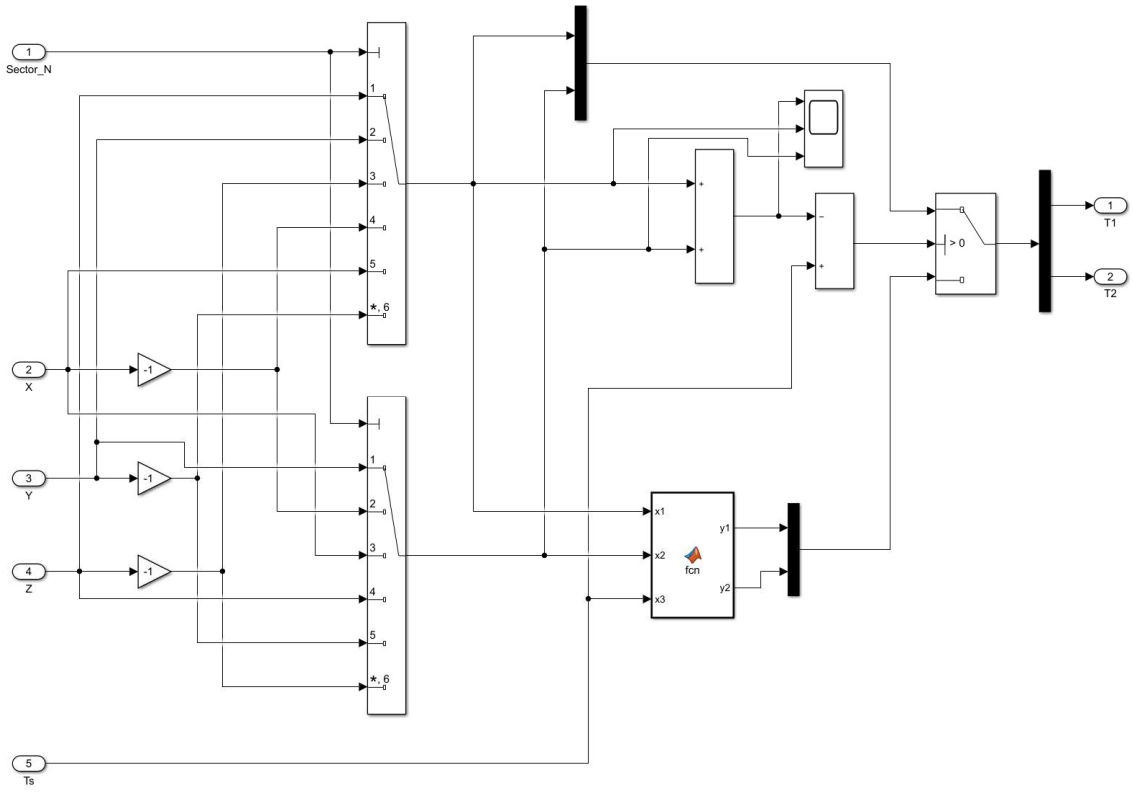

Figure 4.19 Adjacent vectors operation time calculator subsystem

4. Switching time calculator subsystem

Figure 4.20 shows switching time calculator subsystem.

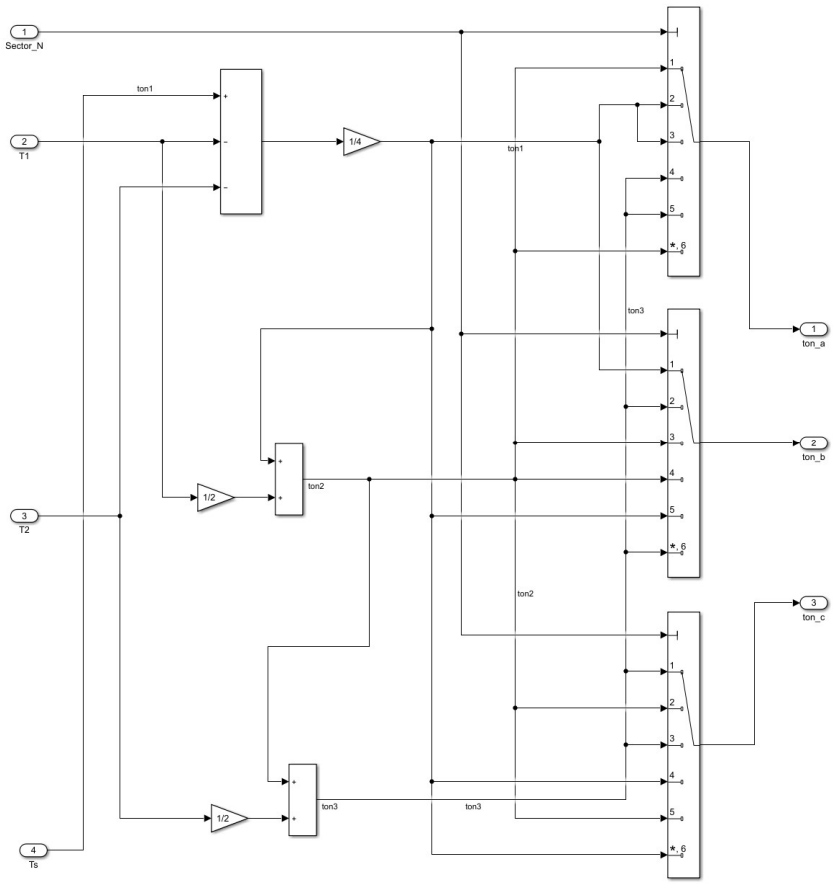

Figure 4.20 Switching time calculator subsystem

4.2 DC output voltages, their dynamic performance on the three methods and the power factor

The dynamic performance is tested on the condition that the initial output voltage is 300 V, the setting voltage is 360 V, at time 0.3 second, a resistive load of 200 ohms is switched in parallel with the original load of 100 ohms, which demands a 1.5 times power than before, at time 0.55 second, this later switched in load is removed, at time 0.8 second,

the Grid side voltage amplitude falls to 0.85 times of the original one and at time 1 second it recovers to the original amplitude.

Figure 4.21 - Figure 4.23 show the dynamic response of the three different control method.

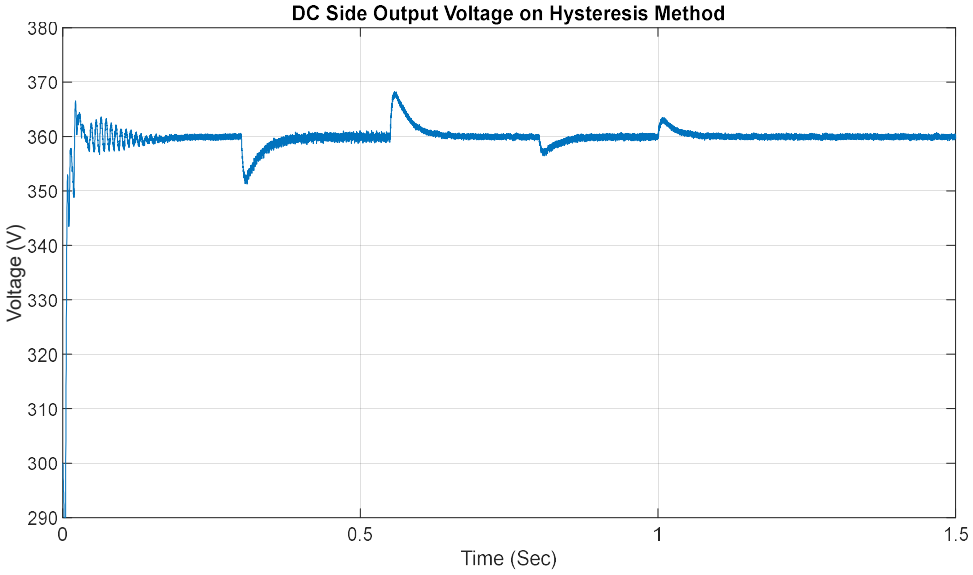

Figure 4.21 The DC side output voltage on Hysteresis method

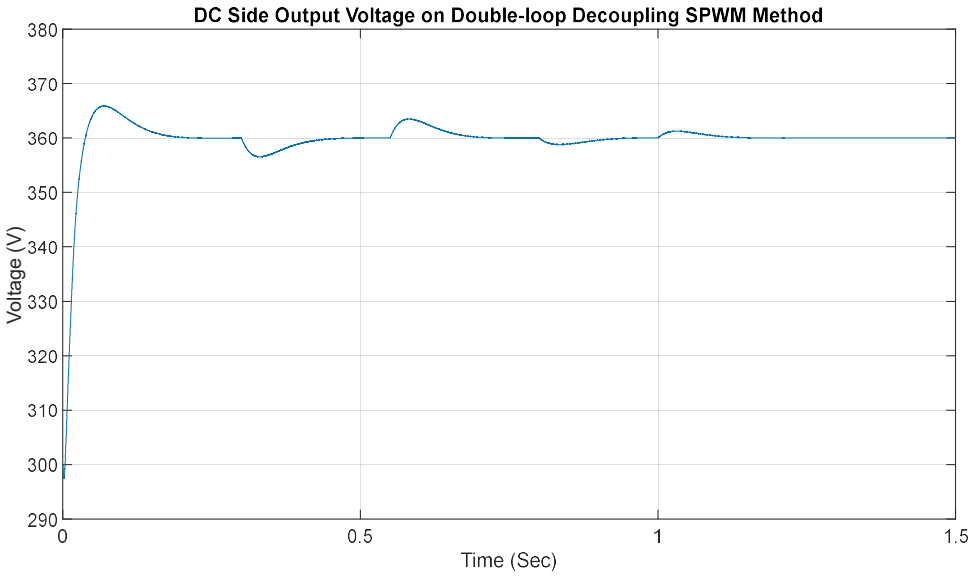

Figure 4.22 The DC side voltage on double-loop decoupling SPWM method

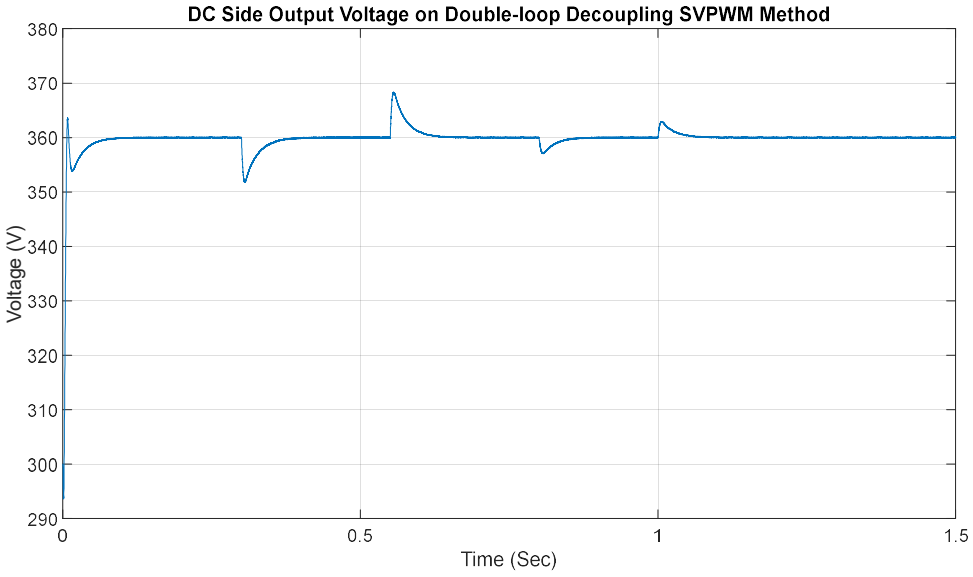

Figure 4.23 The DC side output voltage on double-loop decoupling SVPWM method

Figure 4.24 - Figure 4.26 show the alignments of the AC side three-phase voltage and three-phase current of the three methods, we can see the power factors are close to unity. The currents are enlarged as 17 times as the original currents for better comparison with the voltages.

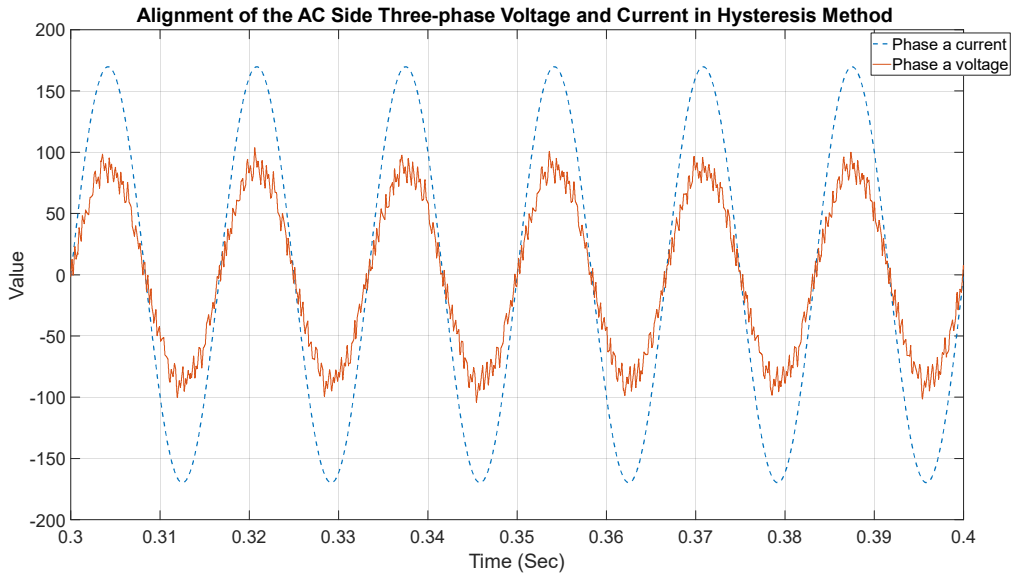

Figure 4.24 Alignment of the AC Side Three-phase Voltage and Current in Hysteresis Method

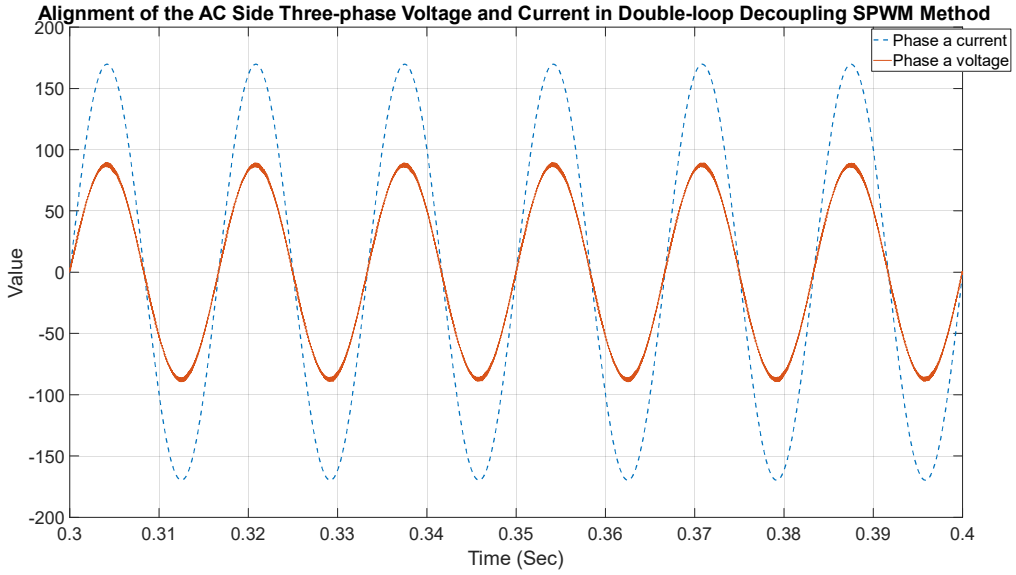

Figure 4.25 Alignment of the AC Side Three-phase Voltage and Current in Double-loop Decoupling SPWM Method

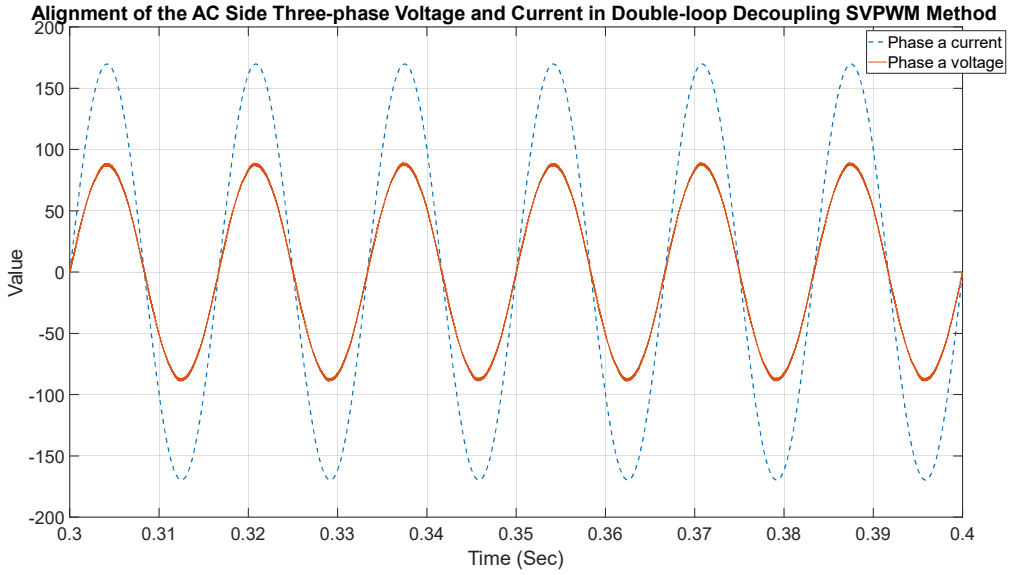

Figure 4.26 Alignment of the AC Side Three-phase Voltage and Current in Double-loop Decoupling SVPWM Method

4.3 Comparisons on power loss of switches

4.3.1 Switch Model

The switches used in the simulation are metal-oxide semiconductor field-effect transistors (MOSFET). The model is shown in Figure 4.27, the setting of parameters is shown in Figure 4.2. The metal-oxide semiconductor field-effect transistor (MOSFET) is a semiconductor device controllable by the gate signal ($g > 0$). The MOSFET device is connected in parallel with an internal diode that turns on when the MOSFET device is reverse biased ($Vds < 0$) and no gate signal is applied ($g=0$). The model is simulated by an ideal switch controlled by a logical signal ($g > 0$ or $g =0$), with a diode connected in parallel. With a positive or negative current flowing through the device, the MOSFET turns off when the gate input becomes 0. If the current I is negative and flowing in the internal diode (no gate signal or $g = 0$), the switch turns off when the current I becomes 0.[30]

Figure 4.28 - Figure 4.31 show an instance of switching on Double-loop decoupling SPWM method, the switch-on time is at 0.408723s, and it finished at time 0.408726s, we ignore the transient process between the two adjacent sample points which are 0.408723s and 0.408726s and assume that the switching process starting at 0.408723s completed at 0.408726s. Before the switching on, the current on the MOSFET is 0, after the switching on, its absolute value rose to 0.7084 A. Before the switching on, the voltage on the MOSFET is 360.008 V. After the switching is completed, the voltage dropped to -

0.0708 V. We use equation (4-7) to calculate the power loss on the switches, where $v_{sw}(t)$ is the voltage on MOSFET and $i_{sw}(t)$ is the current on MOSFET. Since we only sample data at the beginning and end of the switching so there is no data in between, but in the figures, we link the beginning point and the end point with straight lines which are only for linking but do not indicate any real data.

$$P_{sw}(t) = v_{sw}(t)\, i_{sw}(t) \tag{4-7}$$

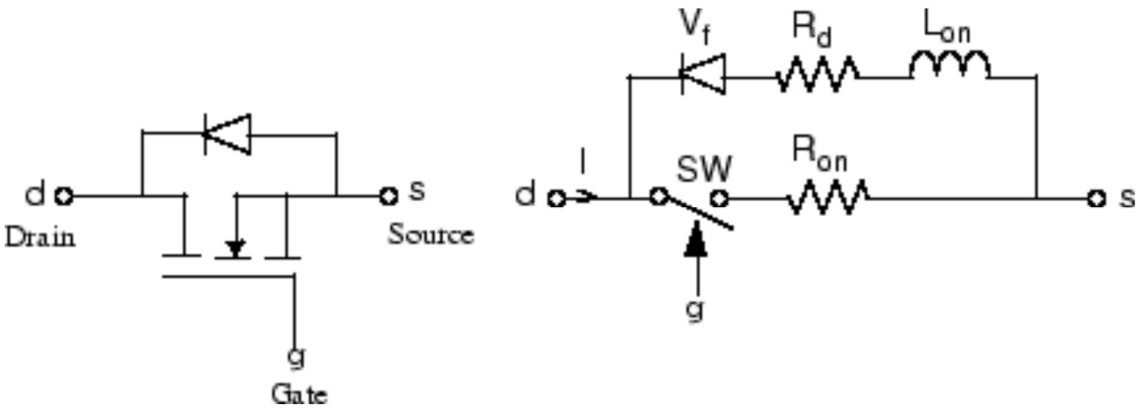

Figure 4.27 Switch Model

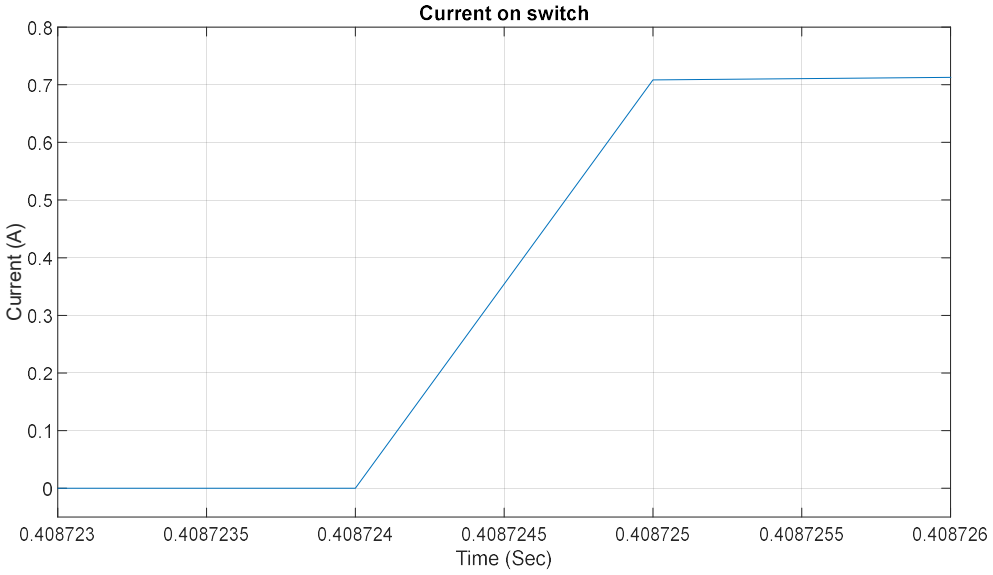

Figure 4.28 Current on MOSFET on switch

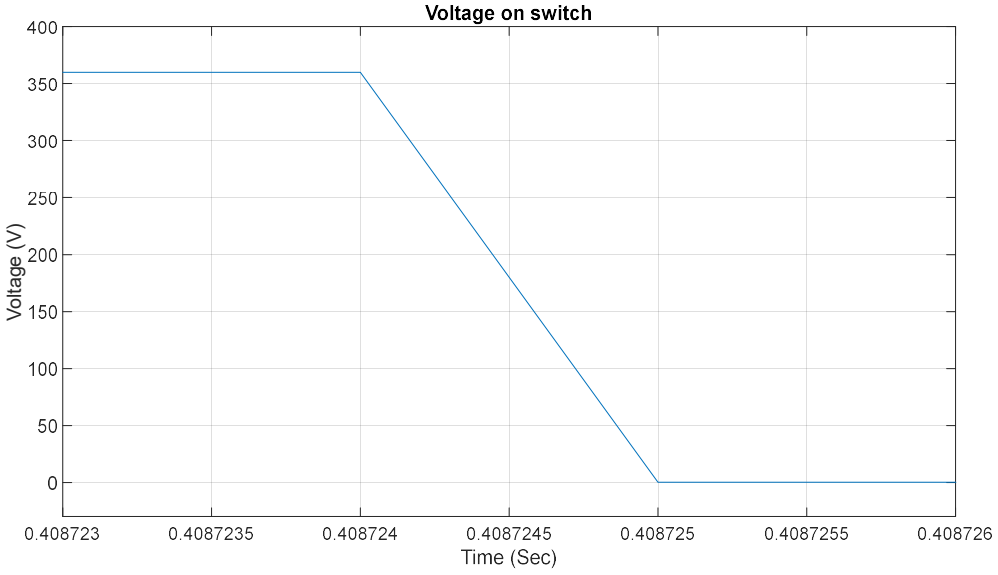

Figure 4.29 Voltage on MOSFET on switch

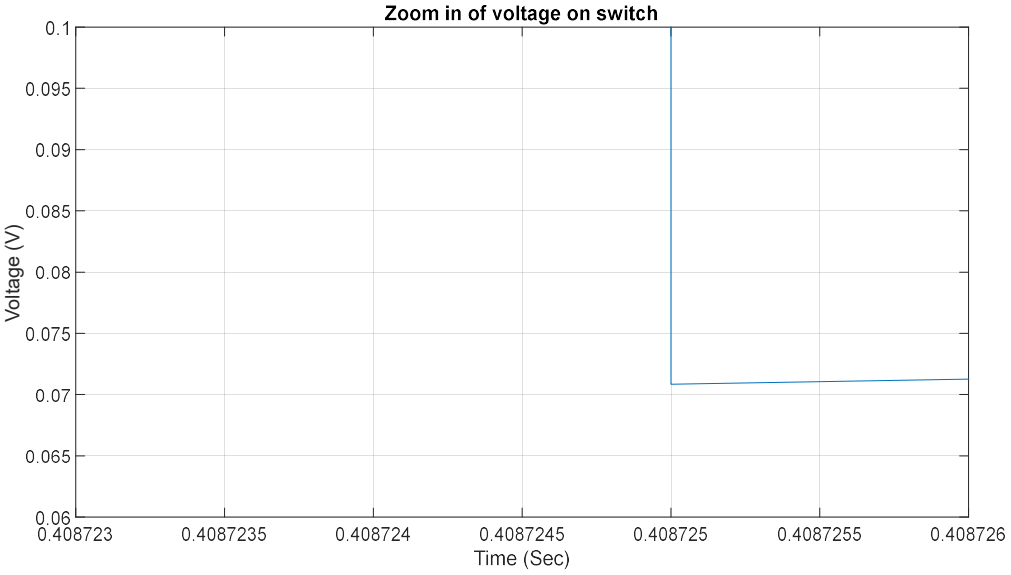

Figure 4.30 Zoom in of Voltage on MOSFET on switch

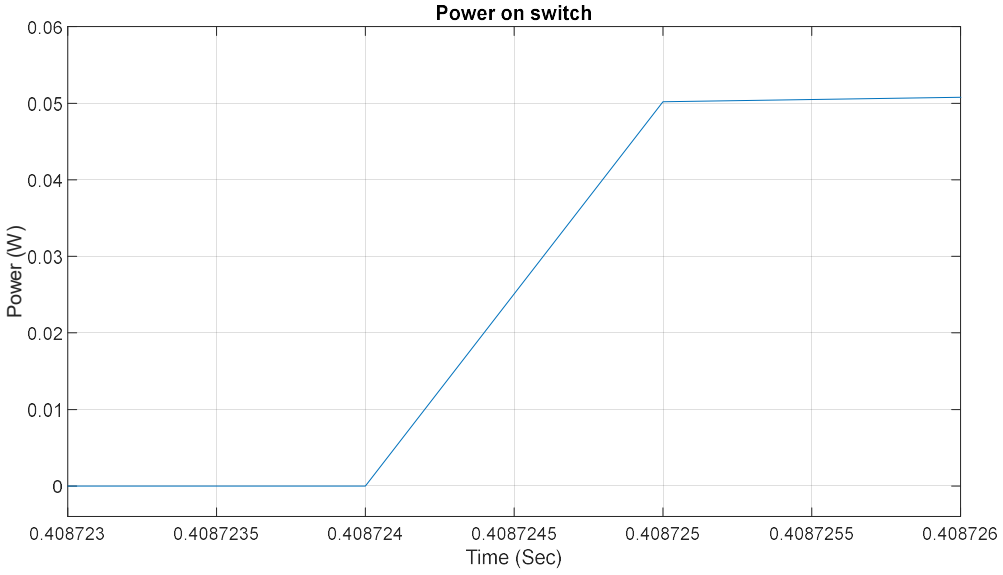

Figure 4.31 Power on MOSFET on switch

4.3.2 Comparison of the Power Loss

Figure 4.32 - Figure 4.34 show the power loss on the switches over a period, the grid side phase-phase voltage amplitude is 220 V, and the DC side resistive load is 100 ohms and there is no change on the grid side voltage and the DC side load. We pick up the start time at time 0.5 s after the system enters the steady state.

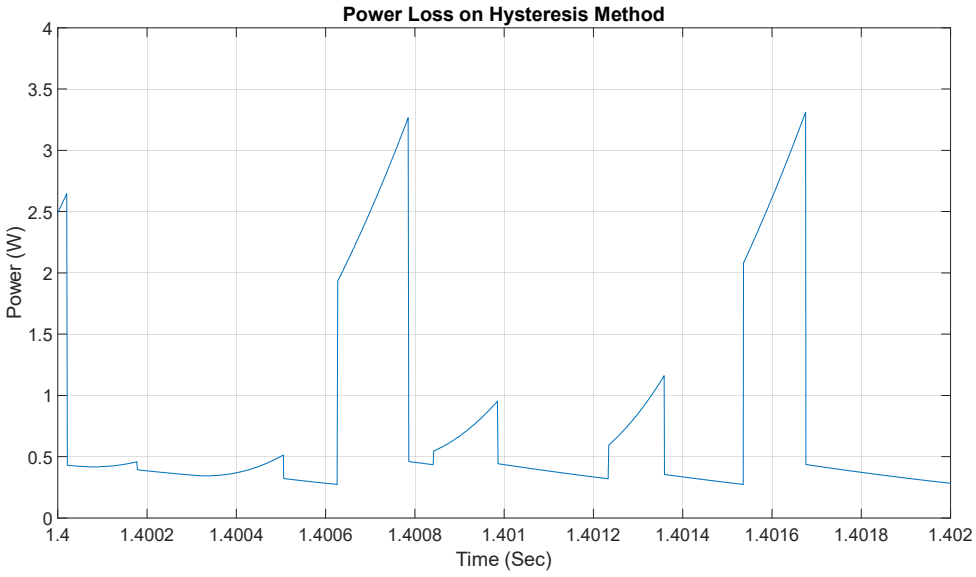

Figure 4.32 Power Loss of Switches on Hysteresis Method

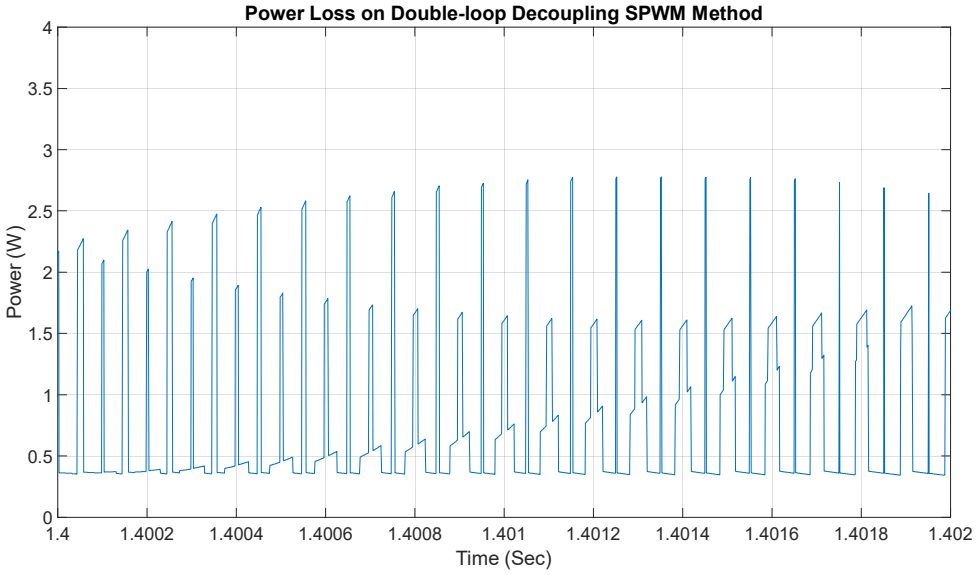

Figure 4.33 Power Loss on Double-loop decoupling SPWM Method

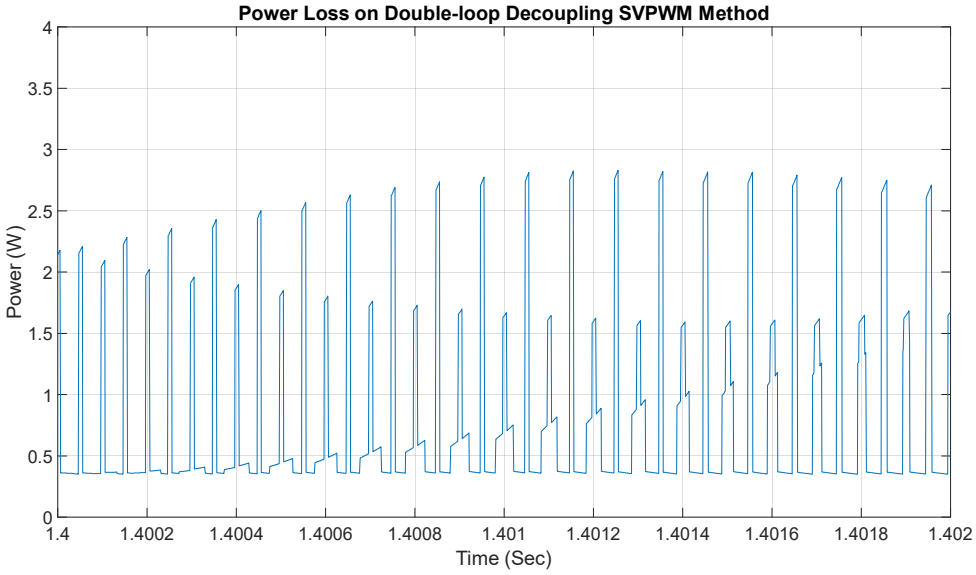

Figure 4.34 Power Loss on Double-loop decoupling SVPWM Method

We use equation (4-8) to calculate the mean power loss.

$$P_{mean} = \frac{1}{t_2 - t_1}\int_{t_1}^{t_2} P_{sw}(t)dt \tag{4-8}$$

where t_1 is the starting time, t_2 is the end time. P_{mean} is the mean power loss of the corresponding method and $P_{sw}(t)$ is the instant power loss on the switch of the corresponding method. We start at the time 0.5s after the system enters the steady state. So, we attain the mean power loss as in Figure 4.35 - Figure 4.37. The mean power loss stabilized around 0.8044 W, 0.7319 W and 0.7798 W in Figure 4.35 - Figure 4.37 respectively. In conclusion, among the three methods, double-loop decoupling SPWM method has the lowest power loss on switches, double-loop, hysteresis method has the second most power loss on switches and double-loop decoupling SVPWM method has the most power loss on switches.

$$\frac{P_{mean\max} - P_{mean\min}}{\left(P_{mean\ Hys} + P_{mean\ SPWM} + P_{mean\ SVPWM}\right)/3} = \frac{0.8044 - 0.7319}{\left(0.8044+0.7319+0.7798\right)/3} = 0.0939 \tag{4-9}$$

where $P_{mean\max}$ is the maximum mean power loss among the three methods, $P_{mean\min}$ is the minimum mean power loss among the three methods, $P_{mean\ Hys}$ is the mean power loss of the hysteresis method, $P_{mean\ SPWM}$ is the mean power loss of the double-loop decoupling SPWM method and $P_{mean\ SVPWM}$ is the mean power loss of the double-loop decoupling SVPWM method.

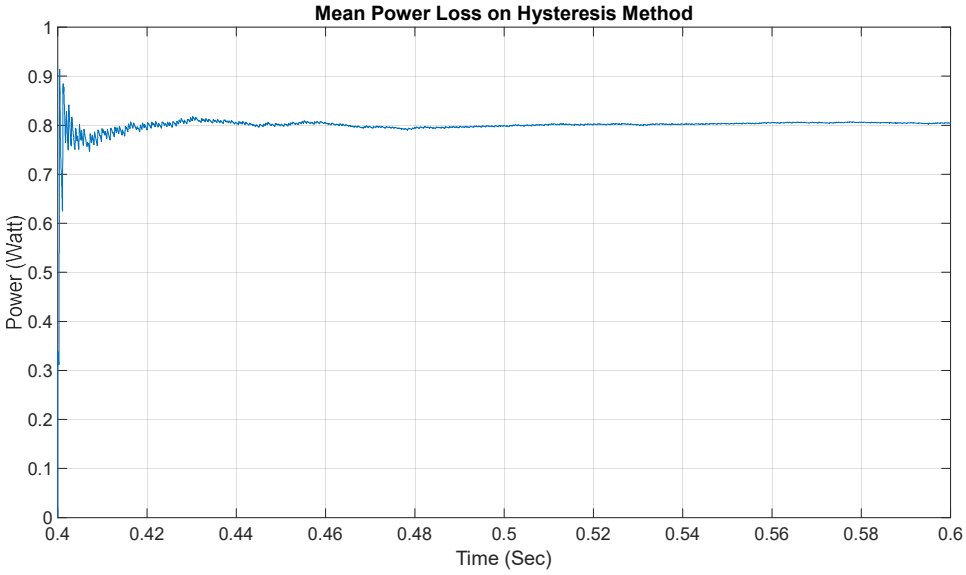

Figure 4.35Mean Power Loss on Hysteresis Method

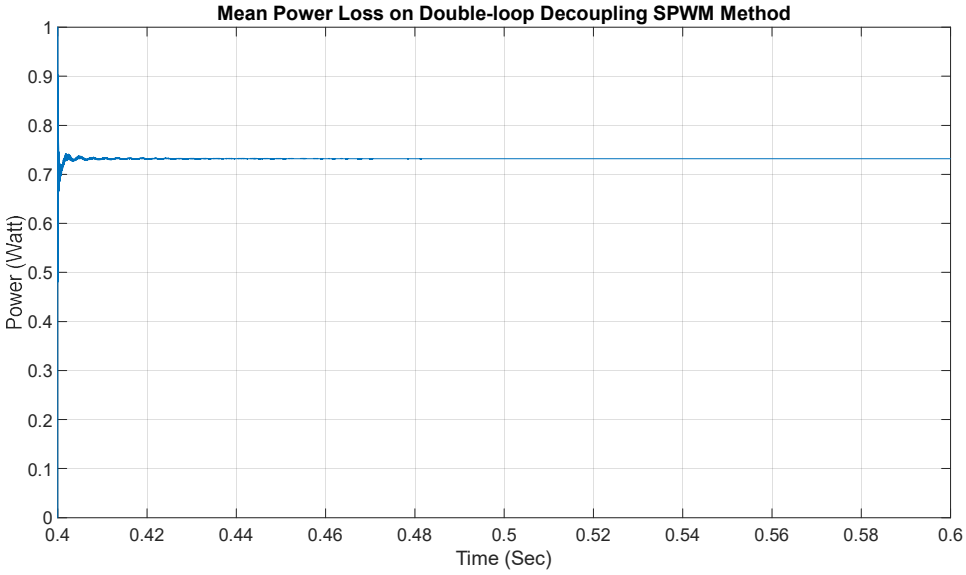

Figure 4.36 Mean Power Loss on Double-loop decoupling SPWM Method

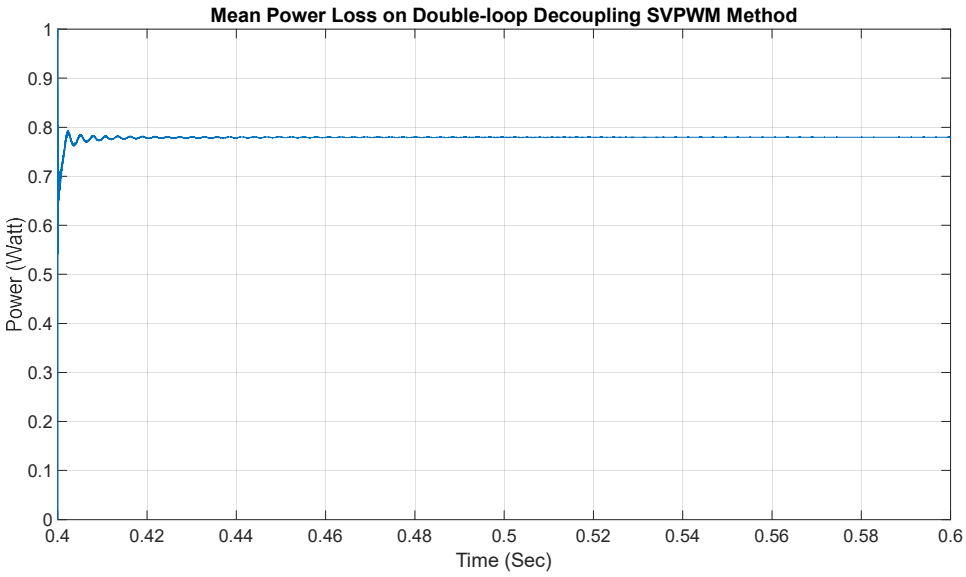

Figure 4.37 Mean Power Loss on Double-loop decoupling SVPWM Method

Chapter 5 Conclusion

Based on the comparison shown in the previous chapter, we can draw the conclusion that in three-phase VSR, double-loop decoupling SPWM method has the lowest power loss on switches, double-loop decoupling SVPWM method has the second less power loss on switches and hysteresis method has the most power loss on switches.

REFERENCES

[1] Entry in Wikipedia: Power Electronics.

[2] Wang Liu. Research on the Key Technology of Three-phase PWM Rectifier Based on SVPWM[D]. Xiangtan University, 2016:1

[3] Kataoka T, et al A pulse-width controlled AC-to-DC converter to improve power factor and waveform of AC line current [J]. IEEE Trans. on Industrial Application, 1979, IA-15(6):670-675.

[4] Buses Alfred, Holtz Joachim. Multiloop control of a unity power factor fast switching AC to DC converter [C]. Proc. Power Electr. Specialist Conf, 1982:171-179.

[5] Akagi Hirofumi et al Instantaneous reactive power compensators comprising switching devices without energy storage components [J]. IEEE Trans. Ind. Appl., 1984, IA-20:625-630.

[6] Green AW, Boys J T, Gates G F. 3-phase voltage sourced reversible rectifier. IEE proceedings 1988, 6(B5):362-370.

[7] Chongwei Zhang, Xing Zhang. PWM rectifier and its control [M]. Beijing: China Machine Press, 2003.

[8] Wang Liu. Research on the Key Technology of Three-phase PWM Rectifier Based on SVPWM[D]. Xiangtan University, 2016:3-4.

[9] Fei Xie. Research on Three-phase Voltage SVPWM Rectifier[D]. Southwest University of Science and Technology, 2019: 3.

[10] Qingshi Zhang. Research on Feedback Linearization Control Method of Voltage Source PWM Rectifier[D]. Thesis for master's degree in Harbin Institute of Technology, 2010:27-41.

[11] Wang Liu. Research on the Key Technology of Three-phase PWM Rectifier Based on SVPWM[D]. Xiangtan University, 2016:7.

[12] Yong Huang. Research and Design of Three-phase Voltage-Source PWM Rectifier[D]. South China University of Technology,2010:10.

[13] Gang Huang. Research on Three-phase High Power Factor PWM Rectifier and Its Control Strategy[D]. Hunan University, 2007: 6-7.

[14] Yong Huang. Research and Design of Three-phase Voltage-Source PWM Rectifier[D]. South China University of Technology,2010:7.

[15] Zhonggang Yin. Research on PWM rectifier based on space voltage vector[D]. Thesis for master's degree in Xi'an University of Technology, 2006.

[16] Yao Jiang. Research on Three-phase Voltage Type PWM Rectifier[D]. Thesis for master's degree in Xi'an University of Technology, 2008.

[17] Zhongliang Huang. DSP-based direct current control voltage type PWM rectifier[D]. Thesis for master's degree in Lanzhou University of Technology, 2006.

[18] Yu Fang. Three-phase PFC and its digital control [D]. Thesis for master's degree in Nanjing University of Aeronautics and Astronautics, 2004.

[19] Yong Huang. Research and Design of Three-phase Voltage-Source PWM Rectifier[D]. South China University of Technology,2010:8-9.

[20] Xing Zhang. Research on PWM rectifier and its control strategy[D]. Hefei University of Technology,2003:33-36.

[21] Entry in Wikipedia: Alpha–beta transformation.

[22] Entry in Wikipedia: Direct-quadrature-zero transformation.

[23] Xing Zhang. Research on PWM rectifier and its control strategy[D]. Hefei University of Technology,2003:42-44.

[24] Fei Xie. Research on Three-phase Voltage SVPWM Rectifier[D]. Southwest University of Science and Technology, 2019: 15.

[25] Yong Huang. Research and Design of Three-phase Voltage-Source PWM Rectifier[D]. South China University of Technology,2010:24.

[26] Yong Huang. Research and Design of Three-phase Voltage-Source PWM Rectifier[D]. South China University of Technology,2010:37-38.

[27] Gang Huang. Research on Three-phase High Power Factor PWM Rectifier and Its Control Strategy) [D]. Hunan University, 2007: 33.

[28] Summary of understanding about SPWM and SVPWM modulation ratio and voltage utilization. Website link: https://blog.csdn.net/sy243772901/article/details/88409975

[29] Fei Xie. Research on Three-phase Voltage SVPWM Rectifier[D]. Southwest University of Science and Technology, 2019: 31-33.

[30] MATLAB Documentation, entry: MOSFET.